

# MmWave UAV Networks with Multi-cell Association: Performance Limit and Optimization

Chun-Hung Liu, Kai-Hsiang Ho and Jwo-Yuh Wu

## Abstract

This paper aims to exploit the fundamental limits on the downlink coverage and spatial throughput performances of a cellular network consisting a tier of unmanned aerial vehicle (UAV) base stations (BSs) using the millimeter wave (mmWave) band and a tier of ground BSs using the ultra high frequency (UHF) band. To reduce handover signaling overhead, the ground BSs take charge of control signaling delivery whereas the UAVs are in charge of payload data transmission so that users need to simultaneously associate with a ground BS and a UAV in this network with a control-data plane-split architecture. We first propose a three-dimensional (3D) location distribution model of the UAVs using stochastic geometry which is able to generally characterize the positions of the UAVs in the sky. Using this 3D distribution model, we propose the multi-cell coverage probability and the volume spectral efficiency of the network, derive their explicit low-complexity expressions and find their upper limits when each of the UAVs and ground BSs is equipped with a massive antenna array. We further show that the multi-cell coverage probability and the volume spectral efficiency can be maximized by optimally deploying and positioning the UAVs in the sky and thereby their fundamental maximal limits are found. These important analytical findings are validated by numerical simulations.

## Index Terms

Unmanned aerial vehicle network, millimeter wave, coverage, throughput, cell association, stochastic geometry

## I. INTRODUCTION

Insatiable mobile throughput demand is the main driver for mobile network operators to adopt millimeter wave (mmWave) spectra that support gigabit connections for data-intensive applications such as virtual reality, augmented reality and immersive gaming. Exploiting the use of the mmWave band may effectively alleviate the spectrum crunch problem in the next generation

C.-H. Liu is with the Department of Electrical and Computer Engineering at Mississippi State University, Mississippi State, USA. K.-H. Ho and J.-Y. Wu are with the institute of Communications Engineering and Department of Electrical and Computer Engineering at National Chiao Tung University, Hsinchu, Taiwan. The corresponding author is Dr. Liu (e-mail: chliu@ece.msstate.edu).

cellular networks. However, its effectiveness may be significantly weakened by environmental blockages thanks to the high path loss and low penetration characteristics of mmWave channels [1]–[3]. A very attractive means of enhancing the propagation performance of the mmWave channels is to use unmanned aerial vehicles (UAVs) equipped with multiple antennas as the “flying” base stations (BSs) using the mmWave band because UAVs are able to agilely position themselves to ameliorate their channel quality in accordance of environmental variations. Due to the mobility of UAVs, UAV-assisted communication techniques will play an important role in cellular networks to fulfill the goals of reliable coverage, high-speed, secure and public safety wireless communications [4] [5].

Despite many of the advantages of UAV communications, to successfully employ UAVs to enhance the performances of cellular networks faces a few practical challenges. First, it should be noticed that UAVs have a limited communication capability owing to their limited size and power. As such, energy-efficient deployment, operation and management are particularly important issues for a cellular network using UAVs as access points or BSs (referred to as a UAV network). Moreover, a UAV network has a highly dynamic network topology due to the high mobility of UAVs so that new communication protocols need to be devised to mitigate the impact of intermittent network connectivity on the network performances. Another fairly challenging issue is how to make UAVs communicate each other and have good backhaul communication mechanisms so that they can be effectively coordinated and scheduled to do cooperative communications, position control, interference management, energy replenishment, etc. [5], [6]. How to tackle these practical networking problems and how the obtained solutions to these problems, if adopted, fundamentally influence the network performances in the network are two paramount questions for the success of UAV networks.

#### *A. Motivation and Prior Work*

In light of these aforementioned issues in mmWave communications and UAV networks, a mmWave UAV network is suggested to adopt a plane-split architecture which has a design of splitting the data and control planes of the cellular networks. Such a plane-split architecture design may considerably reduce the networking complexity of a UAV network, and yet it may incur a more challenging context of network connectivity since users need to reliably and simultaneously connect to a ground terminal/BS taking charge in control signaling and a UAV taking charge in payload data delivery. To the best of our knowledge, the fundamental performances of mmWave UAV networks with a plane-split architecture, such as coverage and spatial network throughput, are not yet addressed and studied in the literature.

There are already a few prior works focusing on the performance analysis of UAV networks. The majority of them particularly studies the coverage performance of UAV networks with different constraints (typically see [7]–[14]). Reference [7], for instance, studied how to optimize the coverage of a single cell by effectively deploying multiple UAVs over the cell. Under a minimal transmit power constraint, an optimal UAV placement algorithm was proposed in [8] to maximize the number of covered users by means of a UAV deployment decoupled in the vertical and horizontal dimensions. The coverage problem of a finite network of UAVs which were modeled as a uniform binomial point process serving a given region was investigated in [9] and the downlink coverage probability of a reference receiver was derived by assuming Nakagami-m fading for all wireless links. For the work in [10], the authors analyzed the coverage performance of UAV-assisted terrestrial cellular networks in which UAVs are randomly deployed in the 3D space with a height constraint, and they then proposed a cooperative UAV clustering scheme to offload traffic from ground BSs to cooperative UAV clusters. Reference [11] studied how to optimize the coverage of a UAV network by fast deploying UAVs in the sky. It considered two fast deployment optimization problems: one is to minimize the maximum deployment delay with fairness consideration and the other is to minimize the total deployment delay with efficiency consideration. The coverage performance of a reference user in a finite network of multiple UAVs was investigated in [13] and a mixed mobility model which characterizes the movement process of a UAV in the 3D cylindrical region was proposed. In addition to the prior works on the coverage problem of UAV networks, there are some other prior works that focused on some special performance metrics of UAV networks. For example, reference [15] proposed a framework for optimizing the performance of finite UAV networks in terms of the average number of bits transmitted to users as well as the flight time of UAVs. Another example is the work in [16] where the secrecy rate performance of a mmWave UAV network modeled by Matérn hardcore point processes was analyzed.

### *B. Contributions*

These aforementioned prior works can provide us with a good picture pertaining to how to use UAV as aerial BSs to improve the performances of cellular networks. Nonetheless, some crucial points in the prior works are not yet adequately in existing studies. For example, the majority of the prior works are built on a simple single cell model with a limited number of UAVs so that their analytical results may not be straightforwardly extended to their corresponding counterpart in a large-scale cellular network with inter-cell interference. Also, most of the prior works consider a fairly simple 3D distribution model of UAVs with a constant height that may not be able to

generally evaluate the performance of UAV networks. Furthermore, the prior works on UAV networks using the mmWave band are still minimal and there seem no prior works focusing on the performance analysis of mmWave UAV networks with a plane-split architecture. Accordingly, the fundamental coverage and throughput performances of multi-cell mmWave UAV networks with a plane-split architecture are still unclear for the time being, which are the main focuses in this paper. The main contributions of this paper are summarized as follows:

- We first propose a mmWave cellular network consisting of one tier of ground BSs which use the UHF band and are in charge of the control signaling plane and one tier of UAV (BSs) that adopt the mmWave band and take charge of the data plane. A 3D random distribution model of the UAVs is also proposed and it is able to generally characterize the positions of the UAVs in the sky.
- Due to the plane-split architecture of the mmWave UAV network, a multi-cell cell association scheme is proposed to help users connect to a ground BS and a UAV at the same time. The multi-cell coverage (probability) and the volume spectral efficiency of the network in the downlink are accordingly proposed as the performance metrics of the mmWave UAV network.
- The explicit and low-complexity expressions of the multi-cell coverage and volume spectral efficiency are derived when all BSs are equipped multiple antennas and their fundamental upper limits are found for the case of massive antenna array.
- We particularly show that the multi-cell coverage and volume spectral efficiency can be maximized by optimizing the intensity and height of the UAVs when all UAVs are controlled at the same height and their fundamental maximal limits are characterized for massive antenna array.
- We also particularly show that the multi-cell coverage does not depend on the intensity of the UAVs and, in addition, the volume spectral efficiency linearly increases with the intensity of the UAVs when all elevation angles from a user to all UAVs remain the same. Under the circumstances, the fundamental maximal limit on the multi-cell coverage can be only achieved by using massive antenna array whereas fundamental maximal limit on the volume spectral efficiency is infinity.

Moreover, some numerical simulation results are provided to validate our analytical findings and observations.

### C. Paper Organization

The rest of this paper is organized as follows. In Section II, we first describe the cellular network model consisting of one tier of mmWave UAVs and one tier of UHF ground BSs and how the UAVs and the ground BSs are distributed in the sky and on the ground, respectively. Section III studies the limit of the multi-cell coverage (probability) and how to maximize it. We then propose the volume spectral efficiency of the mmWave UAV network and analyze its limit in Section IV. Finally, Section V concludes our analytical findings and observations.

## II. SYSTEM MODEL AND PRELIMINARIES

In this paper, we consider a cellular network consisting of two tiers of BSs: a tier of the BSs on the ground and a tier of the UAVs hovering in the sky and serving as aerial BSs. The ground BSs are of the same type and performance, and they are assumed to use the UHF band and form an independent homogeneous Poisson point process (HPPP) of intensity  $\lambda_g$ . In particular, they can be expressed as set  $\Phi_g$  given by

$$\Phi_g \triangleq \{X_{g,i} \in \mathbb{R}^2 : i \in \mathbb{N}_+\}, \quad (1)$$

where  $X_{g,i}$  denotes ground BS  $i$  and its location. Also, we assume all the UAVs are also of the same type and performance and they only use the mmWave band. The ground projection points of the positions of all the UAVs in the sky form an independent HPPP of intensity  $\lambda_u$ . Specifically, the set of all the UAVs is expressed as

$$\Phi_u \triangleq \{U_i \in \mathbb{R}^3 : U_i = (X_{u,i}, H_i), X_{u,i} \in \mathbb{R}^2, H_i \in \mathbb{R}_+, i \in \mathbb{N}_+\}, \quad (2)$$

where  $U_i$  is UAV  $i$  and its location,  $X_{u,i}$  is the ground projection point of  $U_i$ , and  $H_i$  denotes the (random) vertical height of  $U_i$ . This two-tier mmWave UAV network model can be employed in the scenario that the UHF ground BSs have a much higher capability of signal penetration than the mmWave UAVs so that they can be viewed as macro BSs which have much larger transmit power than UAVs and are in charge of the *control signaling plane* of the network to send control signal information to users and UAVs in the network, whereas the UAVs can be viewed as small cell BSs taking charge of the *data plane* of the network to deliver payload data to users since they have a much wider bandwidth than the UHF ground BSs and are able to flexibly adapt their positions to the environment so as to enhance their channel quality. Such a (control-data) plane-split network architecture has the advantage of alleviating the frequent handover problem between small cell BSs [17]. Another feature of this two-tier mmWave UAV network is that it is easily extended to multi-tier planar heterogeneous networks in the literature as long as all the heights of the UAVs are set to zero, which means the modeling and analysis

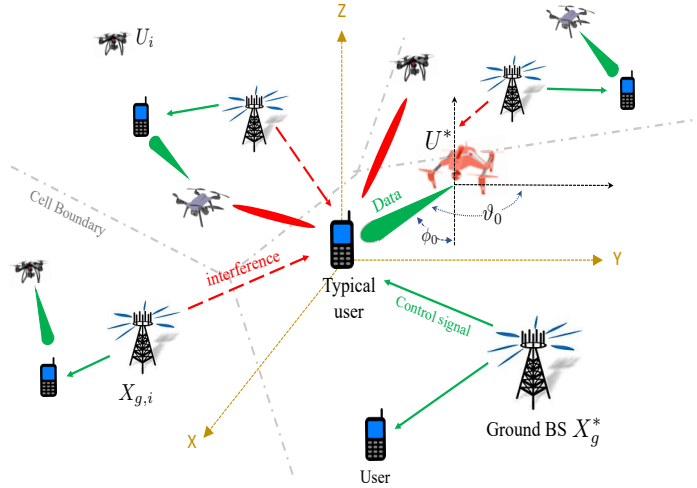


Fig. 1. An illustrative example of a mmWave UAV network with a data-control plane-split architecture. Each user in the network has to associate with a UHF ground BS and a mmWave UAV. Without loss of generality, a typical user is assumed to be located at the origin.

based on the proposed network model in this paper are more general than those in the prior works of multi-tier planar cellular networks. Moreover, all (mobile) users in the network also form an independent HPPP. Without loss of generality, we assume there is a typical user located at the origin and many following equations and analyses will be expressed and proceeded based on the location of this typical user<sup>1</sup>. An illustrative example of the mmWave UAV network with a plane-split architecture is depicted in Fig. 1.

#### A. Elevation Angle, Path-loss Model and Multi-cell Association

A channel in the network is generally considered as either a line-of-sight (LoS) or a non-line-of-sight (NLoS) one. If the channel is visually blocked from a user to a BS, it is NLoS and LoS otherwise. Since whether a channel is LoS or not highly depends on the network environment, we adopt the following low-altitude-platform (LAP) expression in [20] that generally characterizes the LoS probability of a channel between the typical user and UAV  $U_i$  at height  $H_i$  in different network environments:

$$\rho \left( \frac{H_i}{\|X_{u,i}\|} \right) = \left[ 1 + c_2 \exp \left( c_1 \left[ c_2 - \frac{180}{\pi} \tan^{-1} \left( \frac{H_i}{\|X_{u,i}\|} \right) \right] \right) \right]^{-1}, \quad (3)$$

where  $\|X_{u,i}\|$  denotes the Euclidean distance between the typical user and point  $X_{u,i}$ ,  $c_1$  and  $c_2$  are environment-related constants (for rural, urban, etc.) [20]. All  $H_i$ 's for  $i \in \mathbb{N}_+$  are assumed

<sup>1</sup>According to the Slivnyak theorem [18], [19], the statistical properties evaluated at the origin are the same as those evaluated at any particular point in an HPPP.

to be independent random variables (RVs). Note that  $\rho(0) = 1/(1 + c_2 \exp(c_1 c_2)) \triangleq \rho_0$  is not a function of  $H_i$  and  $\|X_{u,i}\|$  any more, i.e., whether the channel between the typical user and a UAV on the ground is LoS does not depend on the distance between them. To generally characterize the position of each UAV in the sky, we propose the following height distribution model of UAV  $U_i$ :

$$H_i \triangleq h_o \|X_{u,i}\|^{-\nu}, \quad (4)$$

where  $h_o \geq 0$  and  $\nu \in \mathbb{R}$  are constants. Namely,  $H_i$  is a power-law function of the distance between the typical user and  $X_{u,i}$  with parameters  $h_o$  and  $\nu$ . Such a height model is motivated by the idea of suppressing the interference, that is, the horizontally farther interfering UAVs can hover either at a lower height to make their channels have a higher NLoS probability or at a higher height to make their channel undergo more path loss. Note that the proposed height distribution is so general that it can characterize many position control scenarios of the UAVs. For the case of  $\nu = 0$ , for instance, all the UAVs are controlled to hover at the same height of  $h_o$ . For the case of  $\nu = -1$ , all the UAVs are controlled to maintain the same elevation angle of  $\tan^{-1}(h_o)$  from the typical user to them. Also note that the heights of the ground BSs are ignored in this paper since they are assumed to be fairly small compared with the heights of the UAVs.

The path-loss model between any BS  $X_i \in \{X_{u,i}, X_{g,i}\}$  and the typical user is given by

$$\xi(\|X_i\|) \triangleq \Psi_i \|X_i\|^\alpha, \quad (5)$$

where  $\alpha \triangleq \alpha_g \mathbf{1}(X_i \in \Phi_g) + \alpha_u \mathbf{1}(X_i \in \Phi_u)$  is the path-loss exponent equal to  $\alpha_g > 2$  if  $X_i \in \Phi_g$  and equal to  $\alpha_u > 2$  if  $X_i \in \Phi_u$ ,  $\mathbf{1}(\mathcal{A})$  is the indicator function that is unity if event  $\mathcal{A}$  is true and zero otherwise,  $\Psi_i \triangleq \Psi_{g,i} \mathbf{1}(X_i \in \Phi_g) + \Psi_{u,i} \mathbf{1}(X_i \in \Phi_u)$  where  $\Psi_{u,i}$  ( $\Psi_{g,i}$ ) is equal to  $\psi_{u,L}$  ( $\psi_{g,L}$ ) if the channel between  $X_i$  and the typical user is LoS and  $\psi_{u,N}$  ( $\psi_{g,N}$ ) otherwise. The physical meaning of  $\psi_{u,L}$  ( $\psi_{g,L}$ ) can be interpreted as the intercept of the LoS mmWave (UHF) channels, whereas the physical meaning of  $\psi_{u,N}$  ( $\psi_{g,N}$ ) can be interpreted as the *integrated intercept and penetration loss* of the NLoS mmWave (UHF) channels [2].

In the light of the plane-split architecture of the cellular network, each user should associate with a ground BS and a UAV at the same time by adopting the following multi-cell association scheme:

$$\begin{cases} X_g^* \triangleq \arg \min_{X_{g,i} \in \Phi_g} \xi(\|X_{g,i}\|) = \arg \min_{X_{g,i} \in \Phi_g} \Psi_{g,i} \|X_{g,i}\|^{\alpha_g} \\ U^* \triangleq \arg \min_{U_i \in \Phi_u} \xi(\|U_i\|) = \arg \min_{U_i \in \Phi_u} \Psi_{u,i} \|U_i\|^{\alpha_u} \end{cases}, \quad (6)$$

where  $X_g^*$  and  $U^*$  denote the ground BS and the UAV associated with the typical user, respec-

tively. Namely, each user associates with the ground BS and the UAV that provide them with the minimum path loss. The path-loss distributions related to  $U^*$  and  $X_g^*$  are given in the following lemma.

**Lemma 1.** *Suppose all the channels between the typical user and the UAVs are spatially independent. If the penetration loss of all NLoS mmWave channels is infinitely large (i.e., considering  $\psi_{u,N} = \infty$ ), then the complementary cumulative distribution function (CCDF) of  $\xi(\|U^*\|)$  in (6) can be found as*

$$\mathbb{P}[\xi(\|U^*\|) \geq x] = \exp\left(-\pi \int_{R(x)} \lambda_u \rho\left(h_o r^{-\frac{(\nu+1)}{2}}\right) dr\right) \quad (7)$$

where  $R(x) \triangleq \{r \in \mathbb{R}_+ : \psi_{u,L}(r + h_o^2 r^{-\nu})^{\frac{\alpha_u}{2}} \leq x\}$ . The CCDF of  $\xi(\|X_g^*\|)$  can be found as

$$\mathbb{P}[\xi(\|X_g^*\|) \geq x] = \exp\left(-\pi \tilde{\lambda}_g x^{\frac{2}{\alpha_g}}\right), \quad (8)$$

where  $\tilde{\lambda}_g \triangleq \lambda_g \left[ \rho_0 \psi_{g,L}^{-\frac{2}{\alpha_g}} + (1 - \rho_0) \psi_{g,N}^{-\frac{2}{\alpha_g}} \right]$  and  $\rho_0 = 1/(1 + c_2 \exp(c_1 c_2))$ .

*Proof:* See Appendix A. ■

Since the link between  $U^*$  and the typical user must be LoS, we know  $\xi(\|U^*\|) = \psi_{u,L} \|U^*\|^{\alpha_u}$ , and thereby (7) leads to the following result:

$$\mathbb{P}[\|U^*\|^2 \leq x] = 1 - \exp\left(-\pi \int_{R(x)} \lambda_u \rho\left(h_o r^{-\frac{(\nu+1)}{2}}\right) dr\right), \quad (9)$$

where  $R(x) = \{r \in \mathbb{R}_+ : (r + h_o^2 r^{-\nu}) \leq x\}$ . This result reveals that the distribution of the square of the distance from the projection point of  $U^*$  to the typical user is characterized by  $\lambda_u \rho(h_o/r^{\frac{(\nu+1)}{2}})$  which can be interpreted as the intensity of the LoS UAVs. Such an LoS UAV intensity is not a constant (except the case of  $\nu = -1$ ) and this means the LoS UAVs in general are a non-homogeneous PPP. We can use two special cases to further explain this interesting and important observation. For example, if  $\nu = 0$ , then all the UAVs are at the height of  $h_o$  in this case, and we thus have

$$\mathbb{P}[\|U^*\|^2 \leq x] = 1 - \exp\left(-\pi \lambda_u \int_0^{(x-h_o^2)^+} \rho\left(\frac{h_o}{\sqrt{r}}\right) dr\right), \quad (10)$$

where  $(x)^+ \triangleq \max\{x, 0\}$ . Thus, all the LoS UAVs with the same height are not an HPPP any more in that their intensity can be equivalently viewed as  $\lambda_u \rho\left(\frac{h_o}{\sqrt{r}}\right)$  which is location-dependent<sup>2</sup>. Another example is the scenario of  $\nu = -1$  in which all the elevation angles from the typical

<sup>2</sup>More precisely, all the UAVs hovering at the same height in the sky form a three-dimensional (3D) non-homogeneous PPP with a location-dependent intensity  $\lambda_u \rho(h_o/\sqrt{r})$ . As such, their ground projection points are a non-homogeneous PPP with the same intensity as well.

user to the LoS UAVs are the same and equal to  $\tan^{-1}(h_o)$  so that we get

$$\mathbb{P} [\|U^*\|^2 \leq x] = 1 - \exp\left(-\frac{\pi\lambda_u\rho(h_o)}{(1+h_o^2)^{\frac{\alpha_u}{2}}}x\right). \quad (11)$$

Hence, all the LoS UAVs form an HPPP of intensity  $\lambda_u\rho(h_o)/(1+h_o^2)^{\frac{\alpha_u}{2}}$  because  $\|U^*\|^2$  is an exponential RV with parameter  $\pi\lambda_u\rho(h_o)/(1+h_o^2)$  [18], [19]. A similar observation can also be drawn for the ground BSs. For example, the result in (8) can alternatively be expressed as

$$\mathbb{P} \left[ [\xi(\|X_g^*\|)]^{\frac{2}{\alpha_g}} \geq x \right] = \exp\left(-\pi\tilde{\lambda}_g x\right), \quad (12)$$

which means that set  $\tilde{\Phi}_g \triangleq \{\tilde{X}_{g,i} : \tilde{X}_{g,i} = \Psi_{g,i}^{\frac{1}{\alpha_g}} X_{g,i}, X_{g,i} \in \Phi_g, \Psi_{g,i} \in \{\psi_{g,L}, \psi_{g,N}\}\}$  can be equivalently viewed as an HPPP of intensity  $\tilde{\lambda}_g$ , as shown in Theorem 1 of our previous work in [21], [22]. The results in Lemma 1 will be employed to exploit the statistical properties of the signal-to-interference plus noise ratio (SINR) of the users in the downlink.

### B. Small-Scale Fading Channel Model with MISO Beamforming

In the previous subsection, the path-loss model between a BS and a user is specified, yet we would like to specify how to model the small-scale multiple-input-single-output (MISO) fading channel gain from a BS to a user in this subsection. For the tractability of analysis, we assume that all the users are equipped with a single antenna, while all the ground BSs and UAVs are equipped with  $N_g$  and  $N_u$  antennas, respectively. Hence, each downlink channel is a MISO channel and the fading channel gain of a channel from BS  $X_i$  to the typical user can be modeled by

$$G_i = G_g^* \mathbb{1}(X_i = X_g^*) + G_{g,i} \mathbb{1}(X_i = X_{g,i} \in \{\Phi_g \setminus X_g^*\}) \\ + \delta_m G_u^* \mathbb{1}(X_i = U^*) + G_{u,i} \mathbb{1}(X_i = U_{u,i} \in \{\Phi_u \setminus U^*\}), \quad (13)$$

where  $G_g^* \sim \text{Gamma}(N_g, N_g)$  denotes the beamforming fading channel gain<sup>3</sup> from  $X_g^*$  and it is a Gamma RV with shape and rate parameters  $N_g$ ,  $G_u^* \sim \text{Gamma}(N_u, N_u)$  is the beamforming fading channel gain<sup>4</sup> from  $U^*$ ,  $G_{g,i} \sim \exp(1)$  is the fading gain from  $X_{g,i}$  which is an exponential RV with unit mean,  $G_{u,i} = \tilde{G}_{u,i}[\delta_m \mathbb{1}(|\vartheta_i| \leq \vartheta_0, |\phi| \leq \phi_0) + \delta_s \mathbb{1}(|\vartheta_i| > \vartheta_0, |\phi_i| \geq \phi_0)]$  denotes the transmit antenna array gain of  $U_i$  in which  $\vartheta_0$  and  $\phi_0$  are the azimuth and the inclination

<sup>3</sup>Please note that the penetration loss of the NLoS channels of the ground BSs is already modeled in their path-loss model so that their fading gain does not need to consider the LoS effect.

<sup>4</sup>According to [23], we know that the fading gain vector of a mmWave multiple-input-multiple-output (MISO) channel can be properly represented by a clustered channel model consisting of small-scale fading and angle-of-departure (AoD)-based transmit array gain vectors. Here we thus assume that all UAVs have a uniform linear array and are able to perfectly align their beam with the angle-of-departure (AoD) of their array in order to maximize their antenna array gain from them to their serving users.

of the main lobe, respectively;  $\vartheta_i$  and  $\phi_i$  are the boresight azimuth and the inclination of  $U_i$ , respectively (see Fig. 1);  $\tilde{G}_{u,i} \sim \exp(1)$ ,  $\delta_m$  and  $\delta_s$  are the main lobe gain and side lobe gain of the antenna array of UAVs, respectively. Note that  $\mathbb{P}[G_{u,i} = \delta_m \tilde{G}_{u,i}] = \frac{\vartheta_0}{2\pi} \times \frac{\phi_0}{\pi}$  and  $\mathbb{P}[G_{u,i} = \delta_s \tilde{G}_{u,i}] = 1 - \frac{\vartheta_0}{2\pi} \times \frac{\phi_0}{\pi}$  since we assume  $\vartheta_i$  is uniformly distributed over  $[-\pi, \pi]$  and  $\phi_i$  is uniformly distributed over  $[-\pi/2, \pi/2]$ . In the following subsection, we will apply the previously proposed path-loss model and the small-scale fading channel model to model two incomplete shot signal processes generated by the UAVs and ground BSs and investigate their statistical properties.

### C. The Incomplete Shot Signal Process

Without loss of generality, we assume that  $U_i \in \Phi_u$  is the UAV that provides the typical user with the  $i$ th smallest path-loss among all the UAVs in  $\Phi_u$ . For the typical user, its 3D  $K$ th-incomplete shot signal process generated by the UAVs in the network is defined as

$$I_{u,K} \triangleq \sum_{i:U_{K+i} \in \Phi_u} \frac{P_u G_{u,K+i}}{\xi(\|U_{K+i}\|)}, \quad (14)$$

where  $P_u$  denotes the transmit power of a UAV. Note that  $I_{u,K}$  does not contain the signal powers generated by the  $K$  UAVs in  $\Phi_u$  that generate the first  $K$  smallest path-loss signals received by the typical user so that it is called the  $K$ th-incomplete shot signal process. Similarly, the path loss from  $X_{g,i}$  to the typical user is assumed to be the  $i$ th smallest one among all the path losses from all the ground BSs in  $\Phi_g$ . We then define the 2D  $K$ th-incomplete shot signal process of the typical user as follows:

$$I_{g,K} \triangleq \sum_{i:X_{g,K+i} \in \Phi_g} \frac{P_g G_{g,K+i}}{\xi(\|X_{g,K+i}\|)} \stackrel{d}{=} \sum_{i:\tilde{X}_{g,K+i} \in \tilde{\Phi}_g} \frac{P_g G_{g,K+i}}{\|\tilde{X}_{g,K+i}\|^{\alpha_g}}, \quad (15)$$

where  $P_g$  is the transmit power of the ground BSs and  $\stackrel{d}{=}$  stands for the equivalence in distribution. Likewise,  $I_{g,K}$  does not include the first  $K$  smallest path-loss signals among all path-loss signals generated by all the ground BSs. Note that we do not consider the void cell phenomenon in (14) and (15) because the user intensity is assumed to be so large that all the UAVs in the network are associated with at least one user with high probability [21], [24].

Studying the statistical properties of  $I_{u,K}$  and  $I_{g,K}$  is crucial because it helps us understand how the aggregated signal powers from the UAVs and the ground BSs are affected by the network parameters (such as LoS/NLoS channel modeling parameters, BS intensities, etc.). In particular, we are interested in the Laplace transforms of  $I_{u,K}$  and  $I_{g,K}$  in that they will facilitate our following analyses. The Laplace transform of a non-negative RV  $Z$  is defined as  $\mathcal{L}_Z(s) \triangleq$

$\mathbb{E}[\exp(-sZ)]$  for  $s > 0$ , and thereby the Laplace transforms of  $I_{u,K}$  and  $I_{g,K}$  are found as shown in the following proposition.

**Proposition 1.** *Suppose all the signal powers from mmWave UAVs with an NLoS channel are so small that they can be completely ignored at the users. According to  $I_{u,K}$  defined in (14) and  $I_{g,K}$  defined in (15), the Laplace transform of  $I_{u,K}$  conditioned on RV  $Y_{u,K}$  can be found as*

$$\mathcal{L}_{I_{u,K}|Y_{u,K}}(s) = \exp \left\{ -\pi \lambda_u \mathfrak{J}_u \left( \frac{s \delta_m P_u}{\psi_{u,L}}, Y_{u,K} \right) \right\}, \quad (16)$$

where the probability density function (PDF) of  $Y_{u,K}$  is given by

$$f_{u,K}(z) = \frac{(\pi \lambda_u)^K [\zeta(z)]^{K-1} \left[ \frac{d\zeta(z)}{dz} \right]}{(K-1)!} e^{-\pi \lambda_u \zeta(z)} \quad (17)$$

in which  $\zeta(z) \triangleq \int_0^z \rho(h_o/r^{\frac{\nu+1}{2}}) dr$  and  $\mathfrak{J}_u(x, y)$  for  $x, y \in \mathbb{R}_+$  is defined as

$$\mathfrak{J}_u(x, y) \triangleq \int_y^\infty \frac{x \rho \left( h_o r^{-\frac{(\nu+1)}{2}} \right)}{\frac{\delta_s}{\delta_m} x + (r + h_o^2 r^{-\nu})^{\frac{\alpha_u}{2}}} \left[ \frac{\delta_s}{\delta_m} + \frac{\vartheta_0 \phi_0 (1 - \frac{\delta_s}{\delta_m})}{2\pi^2} \cdot \frac{(r + h_o^2 r^{-\nu})^{\frac{\alpha_u}{2}}}{[x + (r + h_o^2 r^{-\nu})^{\frac{\alpha_u}{2}}]} \right] dr. \quad (18)$$

The Laplace transform of  $I_{g,K}$  for a given  $Y_{g,K} \sim \text{Gamma}(K, \pi \tilde{\lambda}_g)$  can be derived as

$$\mathcal{L}_{I_{g,K}|Y_{g,K}}(s) = \exp \left[ -\pi \tilde{\lambda}_g Y_{g,K} \mathfrak{J}_g \left( \frac{s P_g}{Y_{g,K}^{\frac{\alpha_g}{2}}}, \frac{2}{\alpha_g} \right) \right], \quad (19)$$

where  $\tilde{\lambda}_g$  is already defined in Lemma 1 and function  $\mathfrak{J}_g(x, y)$  for  $x, y \in \mathbb{R}_+$  is given by

$$\mathfrak{J}_g(x, y) = \int_{x-y}^\infty \frac{x^y}{1+t^{\frac{1}{y}}} dt = x^y \left( \frac{1}{\text{sinc}(y)} - \int_0^{x-y} \frac{dt}{1+t^{\frac{1}{y}}} \right), \quad (20)$$

where  $\text{sinc}(x) \triangleq \frac{\sin(\pi x)}{\pi x}$ . Hence,  $\mathcal{L}_{I_{u,K}}(s) = \mathbb{E}[\mathcal{L}_{I_{u,K}|Y_{u,K}}(s)]$  and  $\mathcal{L}_{I_{g,K}}(s) = \mathbb{E}[\mathcal{L}_{I_{g,K}|Y_{g,K}}(s)]$ .

*Proof:* See Appendix B. ■

The objective of finding the above Laplace transforms of  $I_{u,K}$  and  $I_{g,K}$  is that they can be generally employed in many analytical situations. For example, if users associate with their nearest LoS UAV and they can cancel the signals from the first  $K-1$  nearest interfering LoS UAVs, we can use  $\mathcal{L}_{I_{u,K}}(s)$  to evaluate the statistical properties of the interference from other interfering UAVs so as to clarify the fundamental interplays between the height and intensity of the UAVs. Likewise, the formula of  $\mathcal{L}_{I_{g,K}}(s)$  also helps us characterize the statistical properties of the interference from the ground BSs when the signals from the first  $K$  nearest ground BSs are removed by cell association and/or interference cancellation. Although the results in Proposition 1 are somewhat complex, they are quite general and able to reduce to a much simpler form for some special cases. For example, consider the case of a fixed elevation angle between the typical

user and the UAVs (i.e.,  $\nu = -1$ ) and  $s = \psi_{u,L}(Y_{u,K} + h_o^2 Y_{u,K})^{\frac{\alpha_u}{2}} / \delta_m P_u$  in (16),  $\delta_m \gg \delta_s$  (i.e., the mmWave side-lobe interference is too small to be considered), and (16) then reduces to

$$\mathbb{E} \left[ \mathcal{L}_{I_{u,K}} \left( \frac{\psi_{u,L}(Y_{u,K} + h_o^2 Y_{u,K})^{\frac{\alpha_u}{2}}}{\delta_m P_u} \right) \right] \approx \left( 1 + \frac{\vartheta_0 \phi_0}{2\pi^2} \int_1^\infty \frac{dz}{1 + z^{\frac{\alpha_u}{2}}} \right)^{-K}, \quad (21)$$

which has a closed-form result equal to  $(1 + \frac{\vartheta_0 \phi_0}{8\pi})^{-K}$  if  $\alpha_u = 4$ . This result is not a function of  $\lambda_u$ , i.e., the Laplace transform of  $I_{u,K}$  scaled by  $(Y_{u,K} + h_o^2 Y_{u,K})^{\frac{\alpha_u}{2}}$  does not depend on  $\lambda_u$  any more. Similarly, if  $s = Y_{g,K}^{\frac{\alpha_g}{2}} / P_g$ , then  $\mathcal{L}_{I_{g,K}|Y_{g,K}}(s)$  is largely simplified and  $\mathbb{E}[\mathcal{L}_{I_{g,K}}(s)]$  can be found as a nearly closed-form result given by

$$\mathbb{E} \left[ \mathcal{L}_{I_{g,K}} \left( \frac{Y_{g,K}^{\frac{\alpha_g}{2}}}{P_g} \right) \right] = \left[ 1 + \mathfrak{J}_g \left( 1, \frac{2}{\alpha_g} \right) \right]^{-K}, \quad (22)$$

and it does not depend on the intensity of the ground BSs as well. In other words, the Laplace transform of  $I_{g,K}$  does not change with  $\lambda_g$  if interference  $I_{g,K}$  is scaled by  $Y_{g,K}^{\alpha_g/2}$ . These above observations regarding  $\mathcal{L}_{I_{u,K}}(s)$  and  $\mathcal{L}_{I_{g,K}}(s)$  will be quite useful for the following analyses.

### III. THE MULTI-CELL COVERAGE: LIMIT ANALYSIS AND OPTIMIZATION

In the network, users are able to associate with one ground BS that transmits control signals and one UAV that delivers downlink payload data. Therefore, they have to be simultaneously covered by the two BSs associated with them in order to successfully receive data from their serving UAV. Accordingly, we first propose the SINR models of a user in the mmWave and UHF spectra and use them to define the multi-cell coverage (probability) of a user. Afterwards, we will analyze the multi-cell coverage and study how to maximize it by optimally deploying and positioning the UAVs. Finally, some numerical results are provided to validate our analytical findings and observations.

#### A. Analysis of the Multi-cell Coverage

According to the path-loss model in (5), the multi-cell association scheme in (6), the fading channel gain model in (13), and the  $K$ th-incomplete shot signal process in (14), the SINR of the typical user associating with UAV  $U^*$  is defined as

$$\gamma_u \triangleq \frac{P_u \delta_m G_u^*}{\xi(\|U^*\|)(I_{u,1} + \sigma_u^2)}, \quad (23)$$

where  $\sigma_u^2$  is the noise power in the mmWave band and  $I_{u,1}$  that is the 3D 1st-incomplete shot signal process based on (14) denotes the interference from all the interfering UAVs. Similarly,

the SINR of the typical user associating with ground BS  $X_g^*$  can be defined as

$$\gamma_g \triangleq \frac{P_g G_g^*}{\xi(\|X_g^*\|) I_{g,1}}, \quad (24)$$

where  $I_{g,1}$  is the 2D 1st-incomplete shot signal process accounting for the interference from all the interfering ground BSs. Note that there is no noise power term in (24) because the network in the UHF band is usually interference-limited. Using the SINRs defined in (23) and (24), we can define the *multi-cell coverage* (probability) of a user as follows:

$$p_{cov} \triangleq \mathbb{P}[\min\{\gamma_u, \gamma_g\} \geq \beta] = \mathbb{P}[\gamma_u \geq \beta] \mathbb{P}[\gamma_g \geq \beta] \quad (25)$$

in which  $\beta > 0$  is the SINR threshold for successful decoding. The probability  $\mathbb{P}[\gamma_u \geq \beta] \triangleq p_u$  is called the *UAV coverage*, whereas the probability  $\mathbb{P}[\gamma_g \geq \beta] \triangleq p_g$  is called the *ground coverage*. The equality in (25) holds due to the independence between  $\gamma_u$  and  $\gamma_g$ . This multi-cell coverage reflects how likely a user is able to successfully receive signals from its associated UAV and ground BS at the same time. Such a multi-cell coverage definition stems from the fact that the UAVs can successfully deliver their data to the users in the network only when the users can be simultaneously “covered” by their associated UAV as well as ground BS.

The multi-cell coverage of a user is derived as shown in the following proposition.

**Proposition 2.** *If all the signals from the NLoS UAVs are too small to affect the SINR model in (23) and the multi-cell association scheme in (6) is adopted, the multi-cell coverage defined in (25) can be expressed as  $p_{cov} = p_u p_g$  in which the UAV coverage  $p_u$  can be explicitly found as*

$$p_u = \frac{d^{N_u-1}}{d\tau^{N_u-1}} \left[ \frac{\tau^{N_u-1}}{(N_u-1)!} \int_0^\infty \exp \left\{ -\pi \lambda_u \mathfrak{I}_u \left( \frac{N_u}{\tau} \left( z + \frac{h_o^2}{z^\nu} \right)^{\frac{\alpha_u}{2}}, z \right) - \frac{\psi_{u,L} \sigma_u^2 N_u}{\tau P_u \delta_m} \times \right. \right. \\ \left. \left. \left( z + \frac{h_o^2}{z^\nu} \right)^{\frac{\alpha_u}{2}} \right\} f_{u,1}(z) dz \right] \Big|_{\tau=\frac{1}{\beta}} \quad (26)$$

in which  $f_{u,1}(z)$  is defined in (17) for  $K = 1$  and  $\mathfrak{I}_u(\cdot, \cdot)$  is defined in (18), and the ground coverage  $p_g$  is explicitly derived as

$$p_g = \frac{1}{(N_g-1)!} \frac{d^{N_g-1}}{d\tau^{N_g-1}} \left\{ \frac{\tau^{N_g-1}}{1 + \mathfrak{I}_g \left( \frac{N_g}{\tau}, \frac{2}{\alpha_g} \right)} \right\} \Big|_{\tau=\frac{1}{\beta}}, \quad (27)$$

where  $\mathfrak{I}_g(\cdot, \cdot)$  is defined in (20) and it does not depend on  $\lambda_g$ .

*Proof:* See Appendix C. ■

From Proposition 2, we are able to learn a few important implications which are summarized as follows. First of all, since we devise a new technique to derive the coverage for multiple-

input-single-output (MISO) channels as shown in Appendix C, the two coverage expressions in (26) and (27) are much neater and more general than the existing results of MISO coverage probabilities in the literature (for example, see the coverage results of a mmWave network in [22], [25]). As such, they easily reduce to the results in some special cases. For the single transmit antenna and interference-limited network case, for example,  $p_u$  in (26) significantly reduces to

$$p_u = \int_0^\infty \exp \left\{ -\pi \lambda_u \mathfrak{I}_u \left( \beta \left( z + \frac{h_0^2}{z^\nu} \right)^{\frac{\alpha_u}{2}}, z \right) \right\} f_{u,1}(z) dz, \quad (28)$$

while  $p_g$  in (27) neatly simplifies to

$$p_g = \frac{1}{1 + \mathfrak{I}_g \left( \beta, \frac{2}{\alpha_g} \right)}. \quad (29)$$

Moreover,  $p_u$  in (26) can readily reduce to the coverage for the noise-limited case by setting  $\vartheta_0$  or  $\phi_0$  as zero, and it can also be applied to evaluate the coverage for the case of ground mmWave BSs by setting  $h_o$  equal to zero. Second of all, if all the UAVs and ground BSs are equipped with a massive antenna array and the network is interference-limited, we can further show that  $p_u$  and  $p_g$  in this case can be characterized by the following two expressions:

$$p_u^\infty \triangleq \lim_{N_u \rightarrow \infty} p_u = \int_0^{\beta^{-1}} \mathcal{L}^{-1} \left\{ \int_0^\infty \exp \left[ -\pi \lambda_u \mathfrak{I}_u \left( s \left( z + \frac{h_o^2}{z^\nu} \right)^{\frac{\alpha_u}{2}}, z \right) \right] f_{u,1}(z) dz \right\} (\tau) d\tau \quad (30)$$

and

$$p_g^\infty \triangleq \lim_{N_g \rightarrow \infty} p_g = \int_0^{\beta^{-1}} \mathcal{L}^{-1} \left\{ \left( 1 + \int_1^\infty \frac{s}{s + x^{\frac{\alpha_g}{2}}} dx \right)^{-1} \right\} (\tau) d\tau, \quad (31)$$

where  $\mathcal{L}^{-1}\{f(s)\}(\tau)$  represents the inverse Laplace transform of function  $f(s)$ . *To the best of our knowledge,  $p_u^\infty$  in (30) and  $p_g^\infty$  in (31) are the most explicit coverage expressions firstly found in this paper for mmWave UAV networks with massive MISO beamforming.* They can be effectively evaluated by the numerical techniques of the inverse Laplace transform even though they are not in closed-form. Hence, we conclude that *the upper limit of the multi-cell coverage with massive MISO beamforming is given by*

$$p_{cov}^\infty \triangleq \lim_{N_u, N_g \rightarrow \infty} p_u p_g = p_u^\infty p_g^\infty, \quad (32)$$

which can be analytically evaluated by using (30) and (31). Third of all, since  $p_g$  does not depend on the intensity of the ground BSs, the multi-cell coverage  $p_{cov}$  is only influenced by the intensity and position of the UAVs that largely affect  $p_u$ . In the following subsection, we will further look into how the intensity and position of the UAVs impact  $p_u$  and discuss how to

optimize them in order to maximize  $p_{cov}$ .

### B. Optimal Deployment and Position Control of UAVs for Maximizing Multi-cell Coverage

In this subsection, our focus is on how to maximize the multi-cell coverage by optimally deploying the ground BSs and UAVs as well as controlling the hovering positions of the UAVs. According to Proposition 2, we are able to see how the height distribution models of the UAVs with different values of  $h_o$  and  $\nu$  in (4) impact the coverage performance of the UAVs. Here we are particularly interested in two height control models of the UAVs, i.e., (constant) height control model and (constant) elevation angle control model. They are elaborated as follows.

1) *Height Control Model*: For this model, all the UAVs are controlled to hover at the same height of  $h_o$ , i.e., letting  $\nu = 0$  in (26). Such a height control model has an advantage, that is, it intrinsically suppresses the interference received by a user because the channels from the UAVs farther to the user not only undergo more path loss but also become NLoS with a higher probability due to the smaller elevation angles from the user to the farther UAVs. Another advantage of this model is to make the analysis of the UAV coverage much more tractable so that we are able to analytically understand how the height of the UAVs influences the UAV coverage performance. To further demonstrate this point, consider  $p_u$  in (26) for  $\nu = 0$  and the interference-limited network case, and we thus get

$$p_u = \frac{d^{N_u-1}}{d\tau^{N_u-1}} \left\{ \frac{\tau^{N_u-1}}{(N_u-1)!} \int_0^\infty \exp \left[ -\pi \lambda_u \mathfrak{J}_u \left( \frac{N_u}{\tau} (z + h_o^2)^{\frac{\alpha_u}{2}}, z \right) \right] f_{u,1}(z) dz \right\} \Big|_{\tau=\frac{1}{\beta}}, \quad (33)$$

which essentially indicates that  $\mathfrak{J}_u(\cdot, \cdot)$  dominates  $p_u$  and it is dominated by  $h_o$ . Since the ground coverage  $p_g$  is not dependable upon  $\lambda_g$ ,  $\lambda_u$  and  $h_o$ , we need to maximize the UAV coverage  $p_u$  by optimizing  $\lambda_u$  and  $h_o$  so as to maximize the multi-cell coverage  $p_{cov}$ . To maximize the UAV coverage, we formulate the following optimization problem:

$$\max_{\lambda_u, h_o} p_u \quad \text{s.t. } \lambda_u > 0, h_o > 0, \quad (34)$$

where  $p_u$  is given in (26). This optimization problem enjoys the following property.

**Proposition 3.** *If all the UAVs are controlled to hover at the same height, there exists a unique optimal intensity of  $\lambda_u^*$  that maximizes the UAV coverage in (26). Likewise, there exists an optimal height of  $h_o^*$  that maximizes the UAV coverage for a given UAV intensity.*

*Proof:* See Appendix D. ■

Proposition 3 reveals an important fact, that is, the multi-cell coverage can be maximized by either optimizing  $\lambda_u$  for a given  $h_o$  or optimizing  $h_o$  for a given  $\lambda_u$ . In addition, Proposition

3 is valid for any number of transmit antennas equipped at the UAVs so that the upper limit of the multi-cell coverage with massive MISO beamforming in (32) also can be maximized by optimizing  $\lambda_u$  and  $h_o$ . Likewise, we can formulate the following optimization problem

$$\max_{\lambda_u, h_o} p_{cov}^\infty, \quad \text{s.t. } \lambda_u > 0, h_o > 0. \quad (35)$$

Solving the above optimization problem and then evaluating  $p_{cov}^\infty$  at the optimal solution pair of  $\lambda_u^*$  and  $h_o^*$  give rise to *the fundamental maximal limit of the multi-cell coverage for the height control model*.

2) *Elevation Angle Control Model*: For this model, all the UAVs are controlled to maintain the same elevation angle from the typical user to them, i.e., setting  $\nu = -1$  in (26) makes all the elevation angles from the typical user to all the UAVs equal to  $\tan^{-1}(h_o)$ . Although such an elevation angle control model may not increase the NLoS probability of the channels from all the interfering UAVs to the typical user, it may make the channels of all the interfering UAVs undergo more path loss if compared with the constant height model, especially when the network is in an environment with a large path-loss exponent. By considering the interference-limited case and using (26) with  $\nu = -1$ , the UAV coverage for this elevation angle control model is readily obtained as

$$p_u = \frac{1}{(N_u - 1)!} \frac{d^{N_u-1}}{d\tau^{N_u-1}} \left[ \frac{\tau^{N_u-1}}{\mathfrak{I}_u\left(\frac{N_u}{\tau}(1 + h_o^2)^{\frac{\alpha_u}{2}}, 1\right)/\rho(h_o) + 1} \right] \Big|_{\tau=\frac{1}{\beta}}, \quad (36)$$

which does not depend on the UAV intensity. This result manifests that deploying many UAVs does not ameliorate the UAV coverage once all elevation angles from a user to all the UAVs remain the same. Consequently, the UAVs can only rely on their massive antenna array to further ameliorate  $p_u$ , that is, as  $N_u$  goes to infinity,  $p_u$  in (36) will converge up to

$$p_u^\infty = \lim_{N_u \rightarrow \infty} p_u = \int_0^{\beta^{-1}} \mathcal{L}^{-1} \left\{ \left[ \frac{\mathfrak{I}_u\left(s(1 + h_o^2)^{\frac{\alpha_u}{2}}, 1\right)}{\rho(h_o)} + 1 \right]^{-1} \right\} (\tau) d\tau, \quad (37)$$

which is obtained by using (30) with  $\nu = -1$ . Furthermore, since we can show that  $\mathfrak{I}_u\left(\frac{N_u}{\tau}(1 + h_o^2)^{\frac{\alpha_u}{2}}, 1\right)/\rho(h_o)$  does not depend on  $h_o$  any more, we know that  $p_u$  in (36) and  $p_u$  in (37) cannot be maximized by optimizing  $\lambda_u$  and  $h_o$ . In light of this, it is concluded that  *$p_u$  for the elevation angle control model cannot be maximized by optimizing the UAV intensity and the evaluation angle and it only can be enhanced through massive MISO beamforming so that its fundamental maximal limit is  $p_u^\infty$  in (37)*. Moreover, it is worth pointing out that the height control model may not always outperform the elevation angle control model from the coverage perspective since  $p_u$  in (33) may be smaller than  $p_u$  in (36) for some values of  $\lambda_u$  and  $h_o$ . In the following subsection, we will use some numerical results to verify these aforementioned analytical findings.

TABLE I  
NETWORK PARAMETERS FOR SIMULATION [2], [23]

Parameter \ BS Type	UHF Ground BS	mmWave UAV (28 GHz)
Transmit Power (W) $P_g, P_u$	20	1
Intensity (BSs/m <sup>2</sup> ) $\lambda_g, \lambda_u$	$1 \times 10^{-6}$	$6 \times 10^{-5}$ (or see figures)
Number of Antennas $N_g, N_u$	16	4
Intercept Coefficients (dB) $(\psi_{g u,L}, \psi_{g u,N})$	(37.2, 38.7)	(61.4, 100)
Azimuth of the Main Lobe $\vartheta_0$	(not applicable)	$\frac{2\pi}{3}$
Inclination of the Main Lobe $\phi_0$	(not applicable)	$\frac{1}{3}\pi$
Gain of the Main Lobe $\delta_m$	(not applicable)	1
Gain of the Side Lobe $\delta_s$	(not applicable)	0.1
Maximum Height $h_{\max}$ (m) in (40)	(not applicable)	200
Path-loss Exponent $\alpha_g, \alpha_u$	4	3
Parameters $(c_1, c_2)$ in (3)	(0.16, 9.61)	
SINR Threshold $\beta$	1	

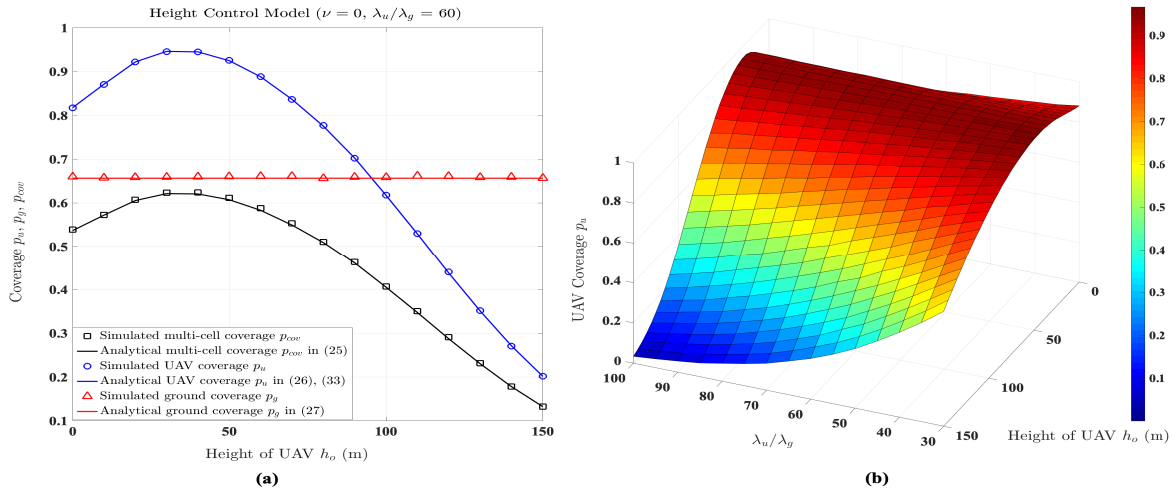


Fig. 2. Simulation results of coverage probabilities  $p_u$ ,  $p_g$  and  $p_{cov}$  for the height control model: (a) Coverage versus Height  $h_o$  of the UAVs for  $\lambda_u/\lambda_g = 60$ , (b) UAV Coverage versus  $\lambda_u/\lambda_g$  and Height  $h_o$  of the UAVs.

### C. Numerical Results

In this subsection, some numerical results are provided to validate our previous analytical results of the multi-cell coverage  $p_{cov}$ , UAV coverage  $p_u$  and ground coverage  $p_g$ . The network parameters for simulation are listed in Table I. To clearly and simply validate our previous analytical results and observations, we consider the mmWave UAV network is so densely deployed that it is interference-limited. We first present the simulation results of the coverage for the height control model in Fig. 2. As shown in Fig. 2(a), we can see how the three different coverage probabilities vary with the height  $h_o$  of the UAVs. All the simulated coverage results perfectly

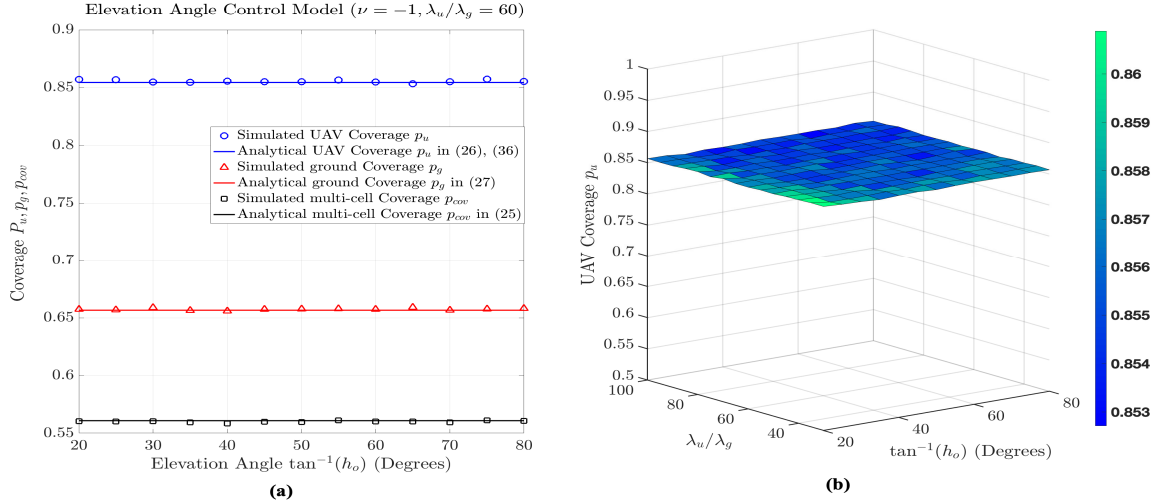


Fig. 3. Simulation results of coverage probabilities  $p_u$ ,  $p_g$  and  $p_{cov}$  for the elevation angle control model: (a) Coverage versus Elevation Angle  $\tan^{-1}(h_o)$  for  $\lambda_u/\lambda_g = 60$ , (b) UAV Coverage versus  $\lambda_u/\lambda_g$  and Elevation Angle  $\tan^{-1}(h_o)$ .

coincide with their corresponding analytical results in Fig. 2(a), which validates the correctness of our previous analyses. The ground coverage, as expected, remains a constant about 0.651, whereas the UAV coverage significantly changes with height  $h_o$  and finally reaches a maximum around 0.95 at  $h_o = 40$  m. Hence, there indeed exists an optimal height that maximizes the UAV coverage, as claimed in Proposition 3, and this phenomenon can also be further observed in Fig. 2(b). From Fig. 2(b), we see how the UAV coverage varies with  $\lambda_u/\lambda_g$  and the height  $h_o$  and how it maximizes at different optimal pairs of  $\lambda_u/\lambda_g$  and  $h_o$ . Since  $p_u$  in general is not a convex function of  $\lambda_u$  and  $h_o$  as shown in Fig. 2(b), there does not exist a unique global pair of  $\lambda_u^*$  and  $h_o^*$  that minimizes  $p_u$ , which supports the statement in Proposition 3.

The simulation results of the coverage probabilities for the elevation angle control model are demonstrated in Fig. 3. The results of the coverage probabilities  $p_u$ ,  $p_g$  and  $p_{cov}$  versus elevation angle  $\tan^{-1}(h_o)$  are shown in Fig. 3(a) and all the analytical results perfectly coincide with their corresponding simulated results. Fig. 3(a) also shows that all the coverage probabilities do not depend the elevation angle  $\tan^{-1}(h_o)$ , which supports our previous discussion. As a matter of fact, all the coverage probabilities are not dependable upon intensity  $\lambda_u$  either. This is demonstrated in 3(b), which plots the UAV coverage  $p_u$  as a 2D horizontal plane located at the height of 0.865. As the figure shows, changing the elevation angle and deploying the UAVs in the sky do not benefit the coverage performance of the users in the network using the elevation angle control model. Hence, if the height of the UAVs is optimally controlled, the height control model certainly outperforms the elevation control model in terms of the UAV coverage, as shown in Fig. 2 and Fig. 3. Fig. 4 shows how the number of the transmit antennas of the UAVs and

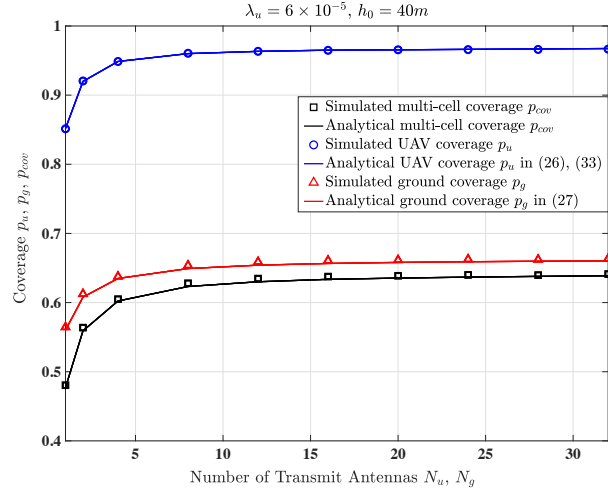


Fig. 4. Simulation results of the coverage probabilities  $p_u$ ,  $p_g$  and  $p_{cov}$  versus the number of transmit antennas  $N_u$  and  $N_g$  for  $\lambda_u/\lambda_g = 60$  and the height control model with  $h_o = 40$  m.

ground BSs impact the coverage probabilities. As shown in the figure, as the numbers of the transmit antennas  $N_u$  and  $N_g$  increase, the UAV coverage and ground coverage increase and eventually converge up to 0.975 and 0.66, respectively. These two maximum coverage values validate the correctness of the upper limits of the UAV coverage in (30) and ground coverage in (31) since they are exactly the same as the coverage values evaluated by (30) and (31).

#### IV. THE VOLUME SPECTRAL EFFICIENCY: LIMIT ANALYSIS AND OPTIMIZATION

In the previous section, we have learned that jointly optimizing the UAV intensity and position is able to maximize the multi-cell coverage. This inspires us to further investigate how the throughput of the UAV mmWave network is affected by the intensity and position of the UAVs. Specifically, we propose the volume spectral efficiency to characterize the network throughput of the UAV mmWave network per unit volume and bandwidth. The volume spectral efficiency will be analyzed and its explicit expression will be derived. We then will study how to maximize the volume spectral efficiency by optimizing the intensity and position of the UAVs.

##### A. Analysis of Volume Spectral Efficiency

Recall that the ground BSs and UAVs are in charge of the control and data planes of the network, respectively. Thus, whether the UAVs are able to effectively deliver data to the users highly depends on whether the users are able to successfully receive the control signals sent by the ground BSs. As a result of this plane-split architecture, the throughput of this mmWave

UAV network needs to consider the ground coverage impact. The link rate from UAV  $U^*$  to the typical user can be characterized by the SINR in (23) and it is defined as

$$C_u \triangleq \log(1 + \gamma_u) \mathbb{1}(\gamma_g \geq \beta), \quad (\text{nats/sec/Hz}), \quad (38)$$

which indicates that  $C_u$  is non-zero if and only if the users are covered by the ground BSs. It can be used to define the *volume spectral efficiency* of the mmWave UAV network as follows:

$$\begin{aligned} V_u &\triangleq \frac{\lambda_u}{h_{\max}} \mathbb{E}[C_u] = \frac{\lambda_u}{h_{\max}} \mathbb{E}[\log(1 + \gamma_u) \mathbb{1}(\gamma_g \geq \beta)] \quad (\text{nats/sec/Hz/m}^3) \\ &= \frac{\lambda_u p_g}{h_{\max}} \mathbb{E}[\log(1 + \gamma_u)], \end{aligned} \quad (39)$$

where  $h_{\max}$  is the maximum height to which each UAV is able to fly up. Obviously,  $V_u$  has the physical meaning of the throughput per unit bandwidth and volume of the network if we interpret  $\lambda_u/h_{\max}$  as the number of the UAVs in a unit volume of the network (i.e., the 3D intensity of the UAVs). An explicit result of  $V_u$  is shown in the following Proposition.

**Proposition 4.** *If the interferences from all the NLoS mmWave channels are so small that they can be ignored in  $\gamma_u$ , then the volume spectral density of the UAV mmWave network is found as*

$$\begin{aligned} V_u &= \frac{\lambda_u p_g}{h_{\max}} \int_{0^+}^{\infty} \frac{1}{s} \left[ 1 - \left( \frac{N_u}{N_u + s} \right)^{N_u} \right] \int_0^{\infty} \exp \left\{ -\pi \lambda_u \mathfrak{I}_u \left( s \left( z + \frac{h_o^2}{z^\nu} \right)^{\frac{\alpha_u}{2}}, z \right) - \right. \\ &\quad \left. s \frac{\psi_{u,L} \sigma_u^2}{P_u \delta_m} \left( z + \frac{h_o^2}{z^\nu} \right)^{\frac{\alpha_u}{2}} \right\} f_{u,1}(z) dz ds. \end{aligned} \quad (40)$$

*If all the UAVs and ground BSs have a massive antenna array (i.e.,  $N_u \rightarrow \infty$  and  $N_g \rightarrow \infty$ ),  $V_u$  in (40) will increase and converge up to*

$$\begin{aligned} V_u^\infty &\triangleq \lim_{N_u, N_g \rightarrow \infty} V_u = \frac{\lambda_u p_g^\infty}{h_{\max}} \int_{0^+}^{\infty} \left( \frac{1 - e^{-s}}{s} \right) \int_0^{\infty} \exp \left\{ -\pi \lambda_u \mathfrak{I}_u \left( s \left( z + \frac{h_o^2}{z^\nu} \right)^{\frac{\alpha_u}{2}}, z \right) - \right. \\ &\quad \left. s \frac{\psi_{u,L} \sigma_u^2}{P_u \delta_m} \left( z + \frac{h_o^2}{z^\nu} \right)^{\frac{\alpha_u}{2}} \right\} f_{u,1}(z) dz ds. \end{aligned} \quad (41)$$

*Proof:* See Appendix E. ■

The expressions of the volume spectral efficiency in (40) and (41) are derived by using the integral identity of Shannon transform in our previous work [26] and they are thus much less complex and more explicit than other expressions in the literature. More importantly, they characterize how the number of the transmit antennas influences the volume spectral efficiency. In addition, Proposition 4 reveals a couple of interesting and crucial facts. We first realize that  $V_u$  does not depend on the intensity of the ground BSs since  $p_g$  is not a function of the intensity of the ground BSs as shown in Proposition 2. The ground BSs are only able to improve  $V_u$  by

using a massive antenna array which makes  $p_g$  increase and eventually converge to (31). The UAVs can improve  $V_u$  by using a massive antenna array as well so that  $V_u$  eventually converges up to  $V_u^\infty$  in (41) *that is the upper limit of the volume spectral efficiency with massive MISO beamforming being employed at all BSs in the network*. We then inspect  $V_u$  in (40) and perceive that  $V_u$  can be also improved through appropriately controlling the intensity and positions of the UAVs, which will be discussed in more detail in the following subsection.

### B. Optimal Deployment and Position Control of UAVs for Maximizing Volume Spectral Efficiency

In this subsection, we focus on the study of maximizing the volume spectral efficiency in (40) by optimizing the UAV intensity  $\lambda_u$  and the parameter  $h_o$  in the height distribution model. In particular, we also consider two position control models of the UAVs, i.e., the height control and elevation control models, as specified in Section III-B. For the interference-limited network with the height control model,  $V_u$  in (40) for  $\nu = 0$  reduces to

$$V_u = \frac{\lambda_u p_g}{h_{\max}} \int_{0^+}^{\infty} \frac{1}{s} \left[ 1 - \left( \frac{N_u}{N_u + s} \right)^{N_u} \right] \int_0^{\infty} e^{-\pi \lambda_u \mathfrak{I}_u \left( s(z+h_o^2)^{\frac{\alpha_u}{2}}, z \right)} f_{u,1}(z) dz ds, \quad (42)$$

which is dominated by  $\lambda_u$  and  $\mathfrak{I}_u \left( s(z+h_o^2)^{\frac{\alpha_u}{2}}, z \right)$ , and thereby  $V_u$  can be maximized by optimizing either  $\lambda_u$  for a given  $h_o$  or  $h_o$  for a given  $\lambda_u$  according to Proposition 2. A similar conclusion can be drawn for  $V_u^\infty$  in (41) as well and thus maximizing  $V_u^\infty$  in (41) over  $\lambda_u$  and  $h_o$  yields the fundamental maximal limit of  $V_u$  for the height control model. For the elevation angle control model,  $V_u$  in (40) for  $\nu = -1$  significantly simplifies to

$$V_u = \frac{\lambda_u p_g}{h_{\max}} \int_{0^+}^{\infty} \frac{1 - \left( \frac{N_u}{N_u + s} \right)^{N_u}}{s \left[ \mathfrak{I}_u \left( s(1+h_o^2)^{\frac{\alpha_u}{2}}, 1 \right) / \rho(h_o) + 1 \right]} ds, \quad (43)$$

which is a linear function of  $\lambda_u$  and not affected by  $h_o$  since  $\mathfrak{I}_u \left( s(1+h_o^2)^{\frac{\alpha_u}{2}}, 1 \right) / \rho(h_o)$ , as discussed in Section III-B, is no longer dependable upon  $h_o$ . On account of this,  $V_u$  in (43) can be ameliorated by increasing  $N_u$  and  $\lambda_u$ , whereas increasing  $\lambda_u$  is a much more efficient means to boost  $V_u$ . This observation importantly reveals that *the volume spectrum efficiency for the elevation height control model can be increasingly improved without a hard limit by continuously deploying UAVs in the sky and its fundamental maximal limit is infinity*. Accordingly, the elevation angle control model outperforms the height control model from the throughput perspective. We will use some numerical results in the following subsection to validate these crucial observations.

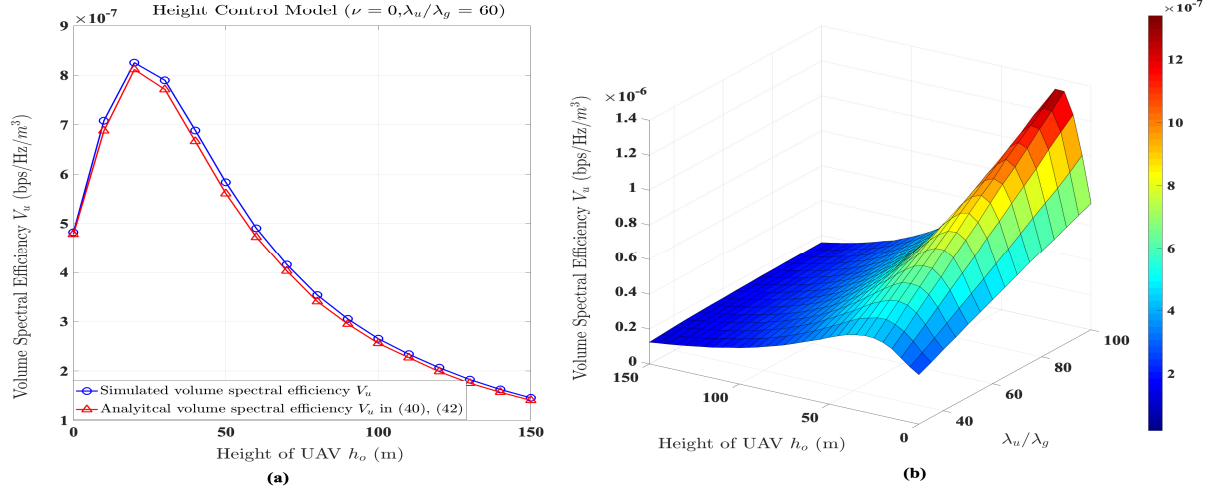


Fig. 5. Simulation results of the volume spectral efficiency for the height control model. (a)  $V_u$  versus height  $h_o$  for  $\lambda_u/\lambda_g = 60$ , (b)  $V_u$  versus Height  $h_o$  (m) and  $\lambda_u/\lambda_g$ .

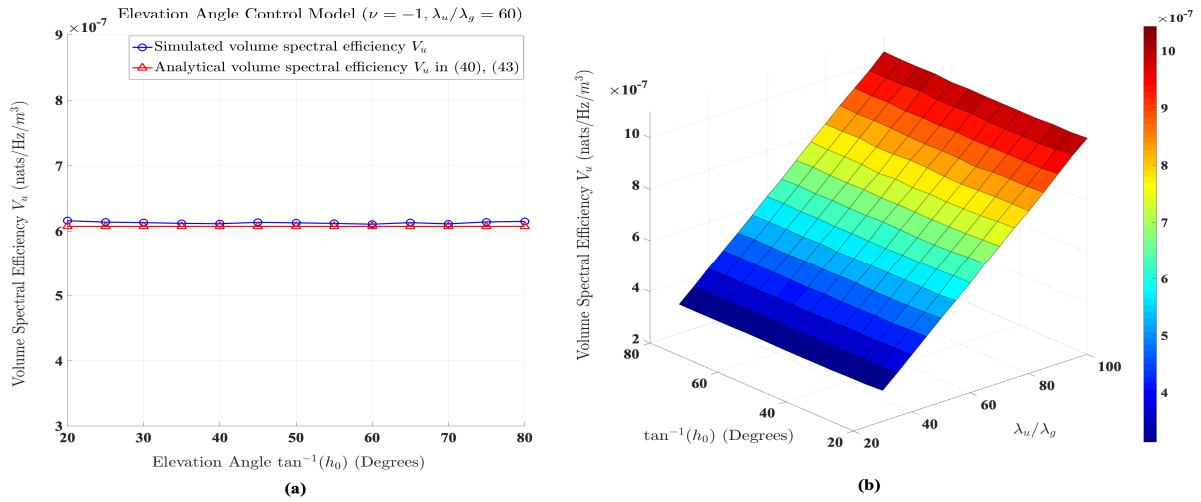


Fig. 6. Simulation results of the volume spectral efficiency for the elevation angle control model. (a)  $V_u$  versus Elevation Angle  $\tan^{-1}(h_o)$  for  $\lambda_u/\lambda_g = 60$ , (b)  $V_u$  versus Elevation Angle  $\tan^{-1}(h_o)$  (Degrees) and  $\lambda_u/\lambda_g$ .

### C. Numerical Results

In this subsection, we would like to demonstrate some numerical results so as to validate our previous analyses pertaining to the volume spectral efficiency  $V_u$ . The network parameters used in this subsection are the same as those in Table I and the network is also considered to be densely deployed and thus interference-limited. The simulation results of the volume spectral efficiency for the height control model are shown in Fig. 5. As can be seen in Fig. 5(a), we first notice that the simulated results perfectly coincide with their analytical results that are obtained

by (42) and thereby the expression in (42) is correct. We also observe that there exists an optimal height around 20 m that maximizes  $V_u$ , and  $V_u$  at the optimal height of 20 m considerably grows by 73% if it is compared with  $V_u$  at the height of zero. Fig. 5(b) shows a 3D plot that depicts how  $V_u$  varies with the elevation angle  $\tan^{-1}(h_0)$  and intensity ratio  $\lambda_u/\lambda_g$ . It essentially verifies our previous conclusion that  $V_u$  can be maximized by optimizing over either height  $h_0$  for a given intensity ratio  $\lambda_u/\lambda_g$  or intensity ratio  $\lambda_u/\lambda_g$  for a given height  $h_0$ . In Fig. 6, we can see the simulation results of the volume spectral efficiency for the elevation angle control model. In particular, Fig. 6(a) presents the numerical results of  $V_u$  versus  $\tan^{-1}(h_0)$  and its simulated results and analytical results obtained by (43) are also very close to each other as well, which validates the correctness of the expression in (43). In addition, we observe Fig. 6(b) and realize that  $V_u$  does not depend on  $\lambda_u/\lambda_g$  and it linearly increases as  $\lambda_u/\lambda_g$  increases, as expected. Hence, the elevation angle control model makes  $V_u$  increase without a hard limit by deploying more and more UAVs, as discussed before.

## V. CONCLUSIONS

In this paper, we aim at the fundamental performance analyses of the multi-cell coverage and volume spectral efficiency of a mmWave UAV network with a plane-split architecture in which users need to associate a ground BS and a UAV to successfully receive data delivered by their associated UAV. We assume the ground BSs form an HPPP and propose a 3D random distribution model of the UAVs that consists of a planar HPPP that describes the ground projection points of the UAVs and a general random height model of the UAVs. Such a 3D distribution model of the UAVs is analytically tractable and first proposed in this paper. The explicit and low-complexity expressions of the multi-cell coverage and volume spectral efficiency are derived by considering the high-penetration-loss characteristic of mmWave channels and their upper limits for the case of massive antenna array beamforming are also characterized. We further show that the multi-cell coverage and volume spectral efficiency can be maximized by means of optimizing the intensity and/or the positions of the UAVs and their fundamental maximal limits can also be accordingly found for massive antenna array.

## APPENDIX

## PROOFS OF LEMMAS AND PROPOSITIONS

## A. Proof of Lemma 1

Since  $\xi(\|U^*\|) = \min_{i:U_i \in \Phi_u} \Psi_{u,i} \|U_i\|^{\alpha_u}$  and all  $\Psi_{u,i}$ 's are independent,  $\mathbb{P}[\xi(\|U_i\|) \geq x]$  can be written as

$$\begin{aligned} \mathbb{P}[\xi(\|U_i\|) \geq x] &= \mathbb{P} \left[ \min_{i:U_i \in \Phi_u} \Psi_{u,i} \|U_i\|^{\alpha_u} \geq x \right] = \mathbb{E} \left\{ \prod_{i:U_i \in \Phi_u} \mathbb{P} \left[ (\|X_{u,i}\|^2 + H_i^2) \geq \left( \frac{x}{\Psi_{u,i}} \right)^{\frac{2}{\alpha_u}} \right] \right\} \\ &\stackrel{(a)}{=} \exp \left( -\pi \lambda_u \int_0^\infty \mathbb{P} \left[ r + h_o^2 r^{-\nu} \leq \left( \frac{x}{\Psi_{u,r}} \right)^{\frac{2}{\alpha_u}} \right] dr \right) \\ &\stackrel{(b)}{=} \exp \left( -\pi \lambda_u \int_0^\infty \rho \left( h_o r^{-\frac{(\nu+1)}{2}} \right) \mathbb{P} \left[ r + h_o^2 r^{-\nu} \leq \left( \frac{x}{\psi_{u,L}} \right)^{\frac{2}{\alpha_u}} \right] dr \right) \\ &\stackrel{(c)}{=} \exp \left( -\pi \lambda_u \int_{R(x)} \rho \left( h_o r^{-\frac{(\nu+1)}{2}} \right) dr \right) \end{aligned}$$

where (a) is obtained by applying the probability generation functional (PGFL) of an HPPP to set  $\{X_{u,i}\}$  that is an HPPP with intensity  $\lambda_u$  and  $H_i = h_o \|X_{u,i}\|^{-\nu}$ , (b) follows from the assumption that the penetration loss of the mmWave channels is infinitely large (i.e.,  $\psi_{u,N} = \infty$ ), and (c) is due to  $R(x) = \{r \in \mathbb{R}_+ : x \geq \psi_{u,L} (r + h_o^2 r^{-\nu})^{\frac{\alpha_u}{2}}\}$ . Hence, the result in (7) is acquired. Next, we find the CCDF of  $\xi(\|X_g^*\|)$  as follows:

$$\begin{aligned} \mathbb{P}[\xi(\|X_g^*\|) \geq x] &= \mathbb{P} \left[ \min_{X_{g,i} \in \Phi_g} \xi(\|X_{g,i}\|) \geq x \right] = \mathbb{E} \left[ \prod_{g,i: X_{g,i} \in \Phi_g} \mathbb{P} [\Psi_{g,i} \|X_{g,i}\|^{\alpha_g} \geq x] \right] \\ &\stackrel{(d)}{=} \exp \left( -\pi \lambda_g \int_0^\infty \mathbb{P} \left[ \Psi_{g,r} \leq x r^{-\frac{\alpha_g}{2}} \right] dr \right) \\ &\stackrel{(e)}{=} \exp \left( -\pi \lambda_g \int_0^\infty \left( \rho_0 \mathbb{P} \left[ r \leq \left( \frac{x}{\psi_{g,L}} \right)^{\frac{2}{\alpha_g}} \right] + (1 - \rho_0) \mathbb{P} \left[ r \leq \left( \frac{x}{\psi_{g,N}} \right)^{\frac{2}{\alpha_g}} \right] \right) dr \right), \quad (\text{A.1}) \end{aligned}$$

where (d) follows from the PGFL of the HPPP  $\Phi_g$  and (e) is obtained by using the assumption that the heights of all the grounds BSs are ignored. Finally, carrying out the integral in (A.1) yields the result in (8).

## B. Proof of Proposition 1

According to Lemma 1, we learn that the LoS UAVs are actually a non-homogeneous PPP with location-dependent intensity  $\lambda_u \rho(h_o/r^{\frac{\nu+1}{2}})$  and we here assume  $X_{u,K}$  is the  $K$ th nearest ground projection point to the typical user among all the projection points of the LoS UAVs.

According to Lemma 1 and (9), we are able to learn that  $\|X_{u,K}\|^2 \stackrel{d}{=} Y_{u,K}$  has the Gamma-RV-based distribution as shown in (17) [19], [27]. Since we know that  $\xi(\|U_i\|) = \Psi_{u,i}\|U_i\|^{\alpha_u} = \Psi_{u,i}^{\frac{2}{\alpha_u}}(\|X_{u,i}\|^2 + h_o^2\|X_{u,i}\|^{-2\nu})$ , the Laplace transform of  $I_{u,K}$  defined in (14) for a given  $Y_{u,K}$ , i.e.,  $\mathcal{L}_{I_{u,K}|Y_{u,K}}(s) \triangleq \mathbb{E}[\exp(-sI_{u,K})|Y_{u,K}]$ , can be rewritten as

$$\begin{aligned} \mathcal{L}_{I_{u,K}|Y_{u,K}}(s) &= \mathbb{E} \left[ \exp \left( -s \sum_{i: X_{u,i} \in \Phi_u \setminus \{X_{u,i}\}_{i=1}^K} \frac{P_u G_{u,i+K}}{\Psi_{u,i+K} (\|X_{u,i+K}\|^2 + h_o^2 \|X_{u,i+K}\|^{-2\nu})^{\frac{\alpha_u}{2}}} \right) \middle| Y_{u,K} \right] \\ &\stackrel{(a)}{=} \mathbb{E}_{\Phi_u} \left[ \prod_{i: X_{u,i} \in \Phi_u} \mathbb{E} \left\{ \exp \left( -s \frac{P_u G_{u,i}}{\Psi_{u,i} (Y_{u,K} + \|X_{u,i}\|^2 + h_o^2 (Y_{u,K} + \|X_{u,i}\|^2)^{-\nu})^{\frac{\alpha_u}{2}}} \right) \right\} \middle| Y_{u,K} \right] \\ &\stackrel{(b)}{=} \exp \left( -\pi \lambda_u \int_{Y_{u,K}}^{\infty} \rho \left( \frac{h_o}{r^{\frac{(\nu+1)}}{2}} \right) \left( 1 - \mathbb{E}_{G_u} \left[ \exp \left( -\frac{s P_u G_u}{\psi_{u,L} (r + h_o^2 r^{-\nu})^{\frac{\alpha_u}{2}}} \right) \right] \right) dr \right), \end{aligned} \quad (\text{A.2})$$

where (a) is obtained by considering  $\|X_{u,K+i}\|^2 \stackrel{d}{=} Y_{u,K} + \|X_{u,i}\|^2$  and the independence between  $Y_{u,K}$  and  $\|X_{u,i}\|^2$  and (b) follows from the result of first applying the probability generating functional (PGFL) of an HPPP to the projection points of  $\Phi_u$  and considering all the NLoS mmWave channels are assumed not to contribute any power to  $I_{u,K}$  (i.e.,  $\psi_{u,N} = \infty$  for all UAVs). Furthermore, we know  $\mathbb{P}[G_u = \tilde{G}\delta_m] = \frac{\vartheta_0\phi_0}{2\pi^2}$  and  $\mathbb{P}[G_u = \tilde{G}\delta_s] = 1 - \frac{\vartheta_0\phi_0}{2\pi^2}$ , and we then have the following result:

$$\begin{aligned} \mathbb{E}_{G_u} \left[ \exp \left( -\frac{s P_u G_u / \psi_{u,L}}{(r + h_o^2 r^{-\nu})^{\frac{\alpha_u}{2}}} \right) \right] &= \left( \frac{\vartheta_0\phi_0}{2\pi^2} \right) \mathbb{E} \left[ \exp \left( -\frac{s P_u \tilde{G}\delta_m}{\psi_{u,L} (r + h_o^2 r^{-\nu})^{\frac{\alpha_u}{2}}} \right) \right] + \left( 1 - \frac{\vartheta_0\phi_0}{2\pi^2} \right) \\ &\times \mathbb{E} \left[ \exp \left( -\frac{s P_u \tilde{G}\delta_s}{\psi_{u,L} (r + h_o^2 r^{-\nu})^{\frac{\alpha_u}{2}}} \right) \right] = \left( \frac{b^{\frac{\alpha_u}{2}}}{\frac{\delta_s}{\delta_m} + b^{\frac{\alpha_u}{2}}} \right) - \left( \frac{\vartheta_0\phi_0}{2\pi^2} \right) \left( \frac{b^{\frac{\alpha_u}{2}} (1 - \delta_s/\delta_m)}{(1 + b^{\frac{\alpha_u}{2}})(\delta_s/\delta_m + b^{\frac{\alpha_u}{2}})} \right), \end{aligned}$$

where  $b = (\frac{\psi_{u,L}}{s P_u \delta_m})^{\frac{2}{\alpha_u}} (r + h_o^2 r^{-\nu})$ . Substituting this result into (A.2) and then performing variable changes in (A.2) yield the result in (16).

Next, we derive the Laplace transform of  $I_{g,K}$  in (15). First, we rewrite  $\mathcal{L}_{I_{g,K}}(s)$  for a given  $Y_{g,K}$  as follows:

$$\begin{aligned} \mathcal{L}_{I_{g,K}|Y_{g,K}}(s) &= \mathbb{E} \left[ \exp \left( -s \sum_{i: \tilde{X}_{g,K+i} \in \tilde{\Phi}_g} \frac{P_g G_{g,K+i}}{\|\tilde{X}_{g,K+i}\|^{\alpha_g}} \right) \right] = \mathbb{E} \left[ \prod_{i: \tilde{X}_{g,i} \in \tilde{\Phi}_g} \exp \left( \frac{-s P_g G_{g,i}}{(Y_{g,K} + \|\tilde{X}_{g,i}\|^2)^{\frac{\alpha_g}{2}}} \right) \right] \\ &\stackrel{(c)}{=} \exp \left\{ -\pi \tilde{\lambda}_g \int_0^{\infty} \left( 1 - \mathbb{E} \left[ \exp \left( -\frac{s P_g G_g}{(Y_{g,K} + r)^{\frac{\alpha_g}{2}}} \right) \right] \right) dr \right\}, \end{aligned} \quad (\text{A.3})$$

where (c) follows from the PGFL of HPPP  $\tilde{\Phi}_g$ ,  $\tilde{\lambda}_g$  is the intensity of  $\tilde{\Phi}_g$ <sup>5</sup>,  $Y_{g,K} \sim \text{Gamma}(K, \pi \tilde{\lambda}_g)$ ,

<sup>5</sup>According to  $\tilde{\Phi}_g$  defined in (15), we thus know its intensity is equal to  $\tilde{\lambda}_g = \lambda_g \mathbb{E}[\Psi_g^{2/\alpha_g}] = \lambda_g [\rho_0 \psi_{g,L}^{2/\alpha_g} + (1 - \rho_0) \psi_{g,N}^{2/\alpha_g}]$  based on the result of Theorem 1 in [21] and  $\mathbb{P}[\Psi_g = \psi_{g,L}] = \rho_0$  as well as  $\mathbb{P}[\Psi_g = \psi_{g,N}] = 1 - \rho_0$ .

and  $G_g \sim \exp(1)$ . Moreover, letting  $W \sim \exp(1)$  yields

$$1 - \mathbb{E} \left[ \exp \left( - \frac{sP_g G_g}{(Y_{g,K} + r)^{\frac{\alpha_g}{2}}} \right) \right] = \mathbb{P} \left[ W \leq \frac{sP_g G_g}{(Y_{g,K} + r)^{\frac{\alpha_g}{2}}} \right] = \mathbb{P} \left[ x \leq \left( \frac{sP_g G_g}{W} \right)^{\frac{2}{\alpha_g}} \right]$$

if  $x \triangleq Y_{g,K} + r$ , which can be used to find the following integral:

$$\begin{aligned} & \int_0^\infty \left( 1 - \mathbb{E} \left[ \exp \left( - \frac{sP_g G_g}{(Y_{g,K} + r)^{\frac{\alpha_g}{2}}} \right) \right] \right) dr = \int_{Y_{g,K}}^\infty \mathbb{P} \left[ x \leq \left( \frac{sP_g G_g}{W} \right)^{\frac{2}{\alpha_g}} \right] dx \\ & = \int_0^\infty \mathbb{P} \left[ x \leq \left( \frac{sP_g G_g}{W} \right)^{\frac{2}{\alpha_g}} \right] dx - \int_0^{Y_{g,K}} \mathbb{P} \left[ x \leq \left( \frac{sP_g G_g}{W} \right)^{\frac{2}{\alpha_g}} \right] dx, \end{aligned} \quad (\text{A.4})$$

where

$$\int_0^\infty \mathbb{P} \left[ x \leq \left( \frac{sP_g G_g}{W} \right)^{\frac{2}{\alpha_g}} \right] dx = \frac{(sP_g)^{\frac{2}{\alpha_g}}}{\text{sinc}(2/\alpha_g)} \quad (\text{A.5})$$

and we also know the following result:

$$\int_0^{Y_{g,K}} \mathbb{P} \left[ x \leq \left( \frac{sP_g G_g}{W} \right)^{\frac{2}{\alpha_g}} \right] dx = \int_0^{Y_{g,K}} \mathbb{P} \left[ W \leq \frac{sP_g G_g}{x^{\frac{\alpha_g}{2}}} \right] dx = \int_0^{\frac{Y_{g,K}}{(sP_g)^{\frac{2}{\alpha_g}}}} \frac{(sP_g)^{\frac{2}{\alpha_g}}}{t^{\frac{\alpha_g}{2}} + 1} dt. \quad (\text{A.6})$$

Substituting (A.5) and (A.6) into (A.4) yields

$$\int_{Y_{g,K}}^\infty \mathbb{P} \left[ x \leq \left( \frac{sP_g G_g}{\Psi_g W} \right)^{\frac{2}{\alpha_g}} \right] dx = Y_{g,K} \mathbb{E} \left[ \mathfrak{J}_g \left( \frac{sP_g}{Y_{g,K}^{\frac{\alpha_g}{2}}}, \frac{2}{\alpha_g} \right) \right],$$

which is then substituted into (A.3), and the result in (20) is obtained.

### C. Proof of Proposition 2

First, we introduce the following identity that holds for a non-negative RV  $Z$ :

$$\mathbb{P}[Z \geq z] = \mathcal{L}^{-1} \left\{ \frac{1}{s} \mathcal{L}_{Z^{-1}}(s) \right\} \left( \frac{1}{z} \right),$$

where  $\mathcal{L}^{-1}\{\cdot\}$  denotes the operator of inverse Laplace transform. Using this identity and the expression in (23) leads to the following expression of  $p_u = \mathbb{P}[\gamma_u \geq \beta]$ :

$$p_u = \mathbb{P}[\gamma_u \geq \beta] = \mathcal{L}^{-1} \left\{ \frac{1}{s} \mathcal{L}_{\gamma_u^{-1}}(s) \right\} \left( \frac{1}{\beta} \right). \quad (\text{A.7})$$

The Laplace transform of  $\gamma_u^{-1}$  can be derived as shown in the following:

$$\begin{aligned} \mathcal{L}_{\gamma_u^{-1}}(s) &= \mathbb{E} \left[ \exp \left( - \frac{s\xi(\|U^*\|)}{P_u \delta_m G_u^*} (I_{u,1} + \sigma_u) \right) \right] \\ &= \mathbb{E} \left[ \mathcal{L}_{I_{u,1}} \left( \frac{s\psi_{u,L}(\|X_u^*\|^2 + h_o^2 \|X_u^*\|^{-2\nu})^{\frac{\alpha_u}{2}}}{P_u \delta_m G_u^*} \right) \cdot \exp \left( - \frac{s\psi_{u,L}(\|X_u^*\|^2 + h_o^2 \|X_u^*\|^{-2\nu})^{\frac{\alpha_u}{2}} \sigma_u^2}{P_u \delta_m G_u^*} \right) \right], \end{aligned}$$

where  $\|X_u^*\|^2 \stackrel{d}{=} Y_{u,1}$  has the distribution in (17) with  $K = 1$ . Next, using (16) in Proposition 1 for given  $\|X_u^*\|^2 = y$  yields the following result:

$$\mathcal{L}_{I_{u,1}|Y_{u,1}} \left( \frac{s\psi_{u,L}(y + h_o^2 y^{-\nu})^{\frac{\alpha_u}{2}}}{P_u \delta_m G_u^*} \right) = \exp \left\{ -\pi \lambda_u \mathfrak{J}_u \left( \frac{s(y + h_o^2 y^{-\nu})^{\frac{\alpha_u}{2}}}{G_u^*}, y \right) \right\}$$

and thereby we have  $\mathcal{L}_{\gamma_u^{-1}}(s) = \mathbb{E} \left[ \exp \left\{ -\tilde{\mathfrak{J}}_u \left( \frac{s}{G_u^*}, Y_{u,1} \right) \right\} \right]$  in which we define  $\tilde{\mathfrak{J}}_u \left( \frac{s}{G_u^*}, Y_{u,1} \right) = -\pi \lambda_u \mathfrak{J}_u \left( s(Y_{u,1} + h_o^2 Y_{u,1}^{-\nu})^{\frac{\alpha_u}{2}} / G_u^*, Y_{u,1} \right) - s\psi_{u,L}(Y_{u,1} + h_o^2 Y_{u,1}^{-\nu})^{\frac{\alpha_u}{2}} \sigma_u^2 / P_u \delta_m G_u^*$  to simplify the expression. In addition, for any positive real-valued function  $\Psi : \mathbb{R}_+ \rightarrow \mathbb{R}_+$  we know the following identity

$$\mathbb{E} \left\{ \frac{1}{s} \exp \left[ -\Psi \left( \frac{s}{Z} \right) \right] \right\} = \int_0^\infty \frac{1}{s} \exp \left[ -\Psi \left( \frac{s}{z} \right) \right] f_Z(z) dz = \int_0^\infty \exp \left[ -\Psi \left( \frac{1}{t} \right) \right] f_Z(st) dt,$$

where  $f_Z(\cdot)$  is the PDF of  $Z$ . By using this identity, we are able to get the following result:

$$\begin{aligned} \frac{1}{s} \mathcal{L}_{\gamma_u^{-1}}(s) &= \mathbb{E} \left[ \frac{1}{s} \exp \left\{ -\tilde{\mathfrak{J}}_u \left( \frac{s}{G_u^*}, Y_{u,1} \right) \right\} \right] \\ &= \frac{N_u^{N_u}}{(N_u - 1)!} \int_0^\infty \mathbb{E}_{Y_{u,1}} \left[ \exp \left\{ -\tilde{\mathfrak{J}}_u \left( \frac{1}{t}, Y_{u,1} \right) \right\} \right] (st)^{N_u-1} e^{-N_u st} dt \\ &= \int_0^\infty \left\{ \frac{1}{(N_u - 1)!} \frac{d^{N_u-1}}{d\tau^{N_u-1}} \mathbb{E}_{Y_{u,1}} \left[ \exp \left\{ -\tilde{\mathfrak{J}}_u \left( \frac{N_u}{\tau}, Y_{u,1} \right) \right\} \tau^{N_u-1} \right] \right\} e^{-s\tau} d\tau \\ &= \mathcal{L} \left\{ \frac{1}{(N_u - 1)!} \frac{d^{N_u-1}}{d\tau^{N_u-1}} \mathbb{E}_{Y_{u,1}} \left[ \exp \left\{ -\tilde{\mathfrak{J}}_u \left( \frac{N_u}{\tau}, Y_{u,1} \right) \right\} \tau^{N_u-1} \right] \right\} (s). \end{aligned} \quad (\text{A.8})$$

Then taking the inverse Laplace transform of the both sides of (A.8) results in

$$\mathcal{L}^{-1} \left\{ \frac{1}{s} \mathcal{L}_{\gamma_u^{-1}}(s) \right\} \left( \frac{1}{\beta} \right) = \frac{1}{(N_u - 1)!} \frac{d^{N_u-1}}{d\tau^{N_u-1}} \mathbb{E} \left\{ \tau^{N_u-1} \exp \left[ -\tilde{\mathfrak{J}}_u \left( \frac{N_u}{\tau}, Y_{u,1} \right) \right] \right\} \Big|_{\tau=\frac{1}{\beta}}$$

and this is exactly the result in (26) because the PDF of  $Y_{u,1}$  is (17) with  $K = 1$ .

By using the above derivation techniques,  $p_g = \mathbb{P}[\gamma_g \geq \beta]$  can first be written as

$$\mathbb{P}[\gamma_g \geq \beta] = \mathcal{L} \left\{ \frac{1}{s} \mathcal{L}_{\gamma_g^{-1}}(s) \right\} \left( \frac{1}{\beta} \right),$$

where  $\mathcal{L}_{\gamma_g^{-1}}(s)$  is

$$\mathcal{L}_{\gamma_g^{-1}}(s) = \mathbb{E} \left[ \exp \left( -s \frac{I_{g,1} \xi(\|X_g^*\|)}{P_g G_g^*} \right) \right] = \mathbb{E} \left[ \mathcal{L}_{I_{g,1} \|\tilde{X}_g^*\|} \left( \frac{s \|\tilde{X}_g^*\|^{\alpha_g}}{P_g G_g^*} \right) \right]. \quad (\text{A.9})$$

According to (20), we can have  $\mathcal{L}_{I_{g,1} \|\tilde{X}_g^*\|}(\cdot)$  given by

$$\mathcal{L}_{I_{g,1} \|\tilde{X}_g^*\|} \left( -\frac{s \xi(\|\tilde{X}_g^*\|)}{P_g G_g^*} \right) = \int_0^\infty \exp \left\{ -\pi \tilde{\lambda}_g \|\tilde{X}_g^*\|^2 \mathfrak{J}_g \left( \frac{s}{y}, \frac{2}{\alpha_g} \right) \right\} f_G(y) dy.$$

Then it follows that

$$\begin{aligned}
\frac{1}{s} \mathcal{L}_{\gamma_g^{-1}}(s) &= \frac{1}{s} \int_0^\infty \mathbb{E} \left\{ \exp \left[ -\pi \tilde{\lambda}_g \|\tilde{X}_g^*\|^2 \mathfrak{I}_g \left( \frac{s}{y}, \frac{2}{\alpha_g} \right) \right] \right\} f_G(y) dy \\
&= \frac{1}{(N_g - 1)!} \int_0^\infty \left[ 1 + \mathfrak{I}_g \left( \frac{N_g}{\tau}, \frac{2}{\alpha_g} \right) \right]^{-1} (s\tau)^{N_g-1} e^{-s\tau} d\tau \\
&= \mathcal{L} \left\{ \frac{1}{(N_g - 1)!} \frac{d^{N_g-1}}{d\tau^{N_g-1}} \left[ \tau^{N_g-1} \left( 1 + \mathfrak{I}_g \left( \frac{N_g}{\tau}, \frac{2}{\alpha_g} \right) \right)^{-1} \right] \right\} (s). \tag{A.10}
\end{aligned}$$

Therefore, taking the inverse Laplace transform of (A.10) results in (27).

#### D. Proof of Proposition 3

For the height control model, the UAV coverage is readily found by letting  $\nu = 0$  in (26) and it is given by

$$p_u = \frac{d^{N_u-1}}{d\tau^{N_u-1}} \left( \frac{\tau^{N_u-1}}{(N_u - 1)!} \int_0^\infty \pi \lambda_u \rho \left( \frac{h_o}{\sqrt{z}} \right) \exp \left\{ -\pi \lambda_u \widehat{\mathfrak{I}}_u(h_o, z) - ax \right\} dz \right) \Big|_{\tau=\frac{1}{\beta}},$$

where  $\widehat{\mathfrak{I}}_u(h_o, z) \triangleq \left[ \int_0^z \rho \left( \frac{h_o}{\sqrt{r}} \right) dr + \mathfrak{I}_u(x, z) \right]$ ,  $x = \frac{N_u}{\tau} (z + h_o^2)^{\frac{\alpha_u}{2}}$  and  $a = \frac{\psi_{u,L} \sigma_u^2}{P_u \delta_m}$ . First, consider the case of a given  $h_o$ . In this case, we know  $\lambda_u \exp[-\pi \lambda_u \widehat{\mathfrak{I}}_u(h_o, z)]$  is a concave function of  $\lambda_u$ . Therefore, there exists a unique optimal value of  $\lambda_u$ , i.e.,  $\lambda_u^*$ , that maximizes  $p_u$ . Next, consider the case of a given  $\lambda_u$ . Since  $\rho(\frac{h_o}{\sqrt{z}})$ ,  $\widehat{\mathfrak{I}}_u(h_o, z)$  and  $x$  all monotonically increase as  $h_o$  increases and we also know the following two asymptotic properties

$$\begin{aligned}
\lim_{h_o \rightarrow 0} \rho \left( \frac{h_o}{\sqrt{z}} \right) \exp \left\{ -\pi \lambda_u \widehat{\mathfrak{I}}_u(h_o, z) - ax \right\} &= \rho_0 \exp \left\{ -\pi \lambda_u \widehat{\mathfrak{I}}_u(0, z) - \frac{aN_u}{\tau} z^{\frac{\alpha_u}{2}} \right\} < \infty \\
\lim_{h_o \rightarrow \infty} \rho \left( \frac{h_o}{\sqrt{z}} \right) \exp \left\{ -\pi \lambda_u \widehat{\mathfrak{I}}_u(h_o, z) - ax \right\} &= 0,
\end{aligned}$$

it follows that  $p_u$  is a continuous and bounded function of  $h_o$ . Also,  $\rho \left( \frac{h_o}{\sqrt{z}} \right) \exp\{-\pi \lambda_u \widehat{\mathfrak{I}}_u(h_o, z) - ax\}$  is not a monotonically decreasing function of  $h_o$ . Letting  $h_o^\dagger$  be the fixed point of the following function G of  $h_o$ :

$$G(h_o) = \rho \left( \frac{h_o}{\sqrt{z}} \right) \exp\{-\pi \lambda_u \widehat{\mathfrak{I}}_u(h_o, z) - ax\} - \rho_0 \exp \left\{ -\pi \lambda_u \widehat{\mathfrak{I}}_u(0, z) - \frac{aN_u}{\tau} z^{\frac{\alpha_u}{2}} \right\}.$$

Hence,  $h_o^\dagger$  exists and  $[0, h_o^\dagger]$  is thus a compact set. Therefore, there exists an optimal height of  $h_o^* \in [0, h_o^\dagger]$  that maximizes  $p_u$  according to the Weierstrass theorem [28].

### E. Proof of Proposition 4

According to (23), the volume spectral efficiency defined in (39) can be expressed as follows:

$$\begin{aligned} V_u &= \frac{\lambda_u}{h_o} p_g \mathbb{E} \left[ \|X_u^*\|^\nu \log \left( 1 + \frac{P_u G_u^* \delta_m}{\psi_{u,L}(\|X_u^*\|^2 + h_0^2 \|X_u^*\|^{-2\nu})^{\frac{\alpha_u}{2}} (I_{u,1} + \sigma_u^2)} \right) \right] \\ &= \frac{\lambda_u}{h_o} p_g \int_0^\infty y^{\frac{\nu}{2}} \mathbb{E} [\log(1 + G_u^* \tilde{\gamma}_u)] \pi \lambda_u e^{-\pi \lambda_u y} dy, \end{aligned} \quad (\text{A.11})$$

where  $\tilde{\gamma}_u \triangleq P_u \delta_m / \psi_{u,L}(y + h_0^2 y^{-\nu})^{\frac{\alpha_u}{2}} (I_{u,1} + \sigma_u^2)$ . Then using Theorem 1 in [26], we can have the following identity:

$$\mathbb{E} [\log(1 + G_u^* \tilde{\gamma}_u)] = \int_{0^+}^\infty \frac{[1 - \mathcal{L}_{G_u^*}(s)]}{s} \mathcal{L}_{\tilde{\gamma}_u^{-1}}(s) ds.$$

From the proof of Proposition 2 in Appendix C, we can infer that  $\mathcal{L}_{\tilde{\gamma}_u^{-1}}(s)$  is given by

$$\mathcal{L}_{\tilde{\gamma}_u^{-1}}(s) = \exp \left[ -\pi \lambda_u \mathcal{J}_u(s(y + h_0^2 y^{-\nu}), y) - s \frac{\psi_{u,L}(y + h_0^2 y^{-\nu}) \sigma_u^2}{P_u \delta_m} \right]$$

Next, since  $G_u^* \sim \text{Gamma}(N_u, N_u)$ , we know  $[1 - \mathcal{L}_{G_u^*}(s)]/s$  can be found as

$$\frac{[1 - \mathcal{L}_{G_u^*}(s)]}{s} = \frac{1}{s} \left[ 1 - \left( \frac{N_u}{N_u + s} \right)^{N_u} \right].$$

Hence, we have

$$\begin{aligned} \mathbb{E} [\log(1 + G_u^* \tilde{\gamma}_u)] &= \int_{0^+}^\infty \frac{1}{s} \left[ 1 - \left( \frac{N_u}{N_u + s} \right)^{N_u} \right] \exp \left\{ -\pi \lambda_u \mathcal{J}_u(s(y + h_0^2 y^{-\nu}), y) \right. \\ &\quad \left. - s \frac{\psi_{u,L} \sigma_u^2}{P_u \delta_m} (y + h_0^2 y^{-\nu}) \right\} ds. \end{aligned} \quad (\text{A.12})$$

Then substituting (A.12) into (A.11) leads to the result in (40).

## REFERENCES

- [1] S. Rangan, T. S. Rappaport, and E. Erkip, "Millimeter-wave cellular wireless networks: Potentials and challenges," *Proc. of The IEEE*, vol. 102, no. 3, pp. 366–385, Mar. 2014.
- [2] T. S. Rappaport, J. George R. MacCartney, M. K. Samimi, and S. Sun, "Wideband millimeter-wave propagation measurements and channel models for future wireless communication system design," *IEEE Trans. Commun.*, vol. 63, no. 9, pp. 3029–3056, Sep. 2015.
- [3] X. Wang, L. Kong *et al.*, "Millimeter wave communication: A comprehensive survey," *IEEE Commun. Surveys Tuts.*, vol. 20, no. 3, pp. 1616–1653, 3rd Quart. 2018.
- [4] Z. Xiao, P. Xia, and X.-G. Xia, "Enabling UAV cellular with millimeter-wave communication: Potentials and approaches," *IEEE Commun. Mag.*, vol. 54, no. 5, pp. 66–73, May 2016.
- [5] A. Fotouhi, H. Qiang *et al.*, "Survey on UAV cellular communications: Practical aspects, standardization advancements, regulation, and security challenges," *IEEE Commun. Surveys Tuts.*, pp. 1–26, Early Access 2019.
- [6] Y. Zeng, R. Zhang, and T. J. Lim, "Wireless communications with unmanned aerial vehicles: Opportunities and challenges," *IEEE Commun. Mag.*, vol. 54, no. 5, pp. 36–42, May 2016.

- [7] M. Mozaffari, W. Saad, M. Bennis, and M. Debbah, "Efficient deployment of multiple unmanned aerial vehicles for optimal wireless coverage," *IEEE Commun. Lett.*, vol. 20, no. 8, pp. 1647–1649, Aug. 2016.
- [8] M. Alzenad, A. El-Keyi, F. Lagum, and H. Yanikomeroglu, "3-D placement of an unmanned aerial vehicle base station (UAV-BS) for energy-efficient maximal coverage," *IEEE Wireless Commun. Lett.*, vol. 6, no. 4, pp. 434–437, Aug. 2017.
- [9] V. V. Chetlur and H. S. Dhillon, "Downlink coverage analysis for a finite 3-D wireless network of unmanned aerial vehicles," *IEEE Trans. Commun.*, vol. 65, no. 10, pp. 4543–4558, Oct. 2017.
- [10] H. Wu, X. Tao *et al.*, "Cooperative UAV cluster-assisted terrestrial cellular networks for ubiquitous coverage," *IEEE J. Sel. Areas Commun.*, vol. 36, no. 9, pp. 2045–2058, Sep. 2018.
- [11] X. Zhang and L. Duan, "Fast deployment of UAV networks for optimal wireless coverage," *IEEE Trans. Mobile Comput.*, vol. 18, no. 3, pp. 588–601, Mar. 2019.
- [12] A. V. Savkin and H. Huang, "Deployment of unmanned aerial vehicle base stations for optimal quality of coverage," *IEEE Wireless Commun. Lett.*, vol. 8, no. 1, pp. 321–324, Feb. 2019.
- [13] P. K. Sharma and D. I. Kim, "Random 3D mobile UAV networks: Mobility modeling and coverage probability," *IEEE Trans. Wireless Commun.*, vol. 18, no. 5, pp. 2527–2538, May 2019.
- [14] M. M. Azari, F. Rosas, and S. Pollin, "Cellular connectivity for uavs: Network modeling, performance analysis and design guidelines," *IEEE Trans. Wireless Commun.*, pp. 1–15, Early Access 2019.
- [15] M. Mozaffari, W. Saad, M. Bennis, and M. Debbah, "Wireless communication using unmanned aerial vehicles (UAVs): Optimal transport theory for hover time optimization," *IEEE Trans. Wireless Commun.*, vol. 16, no. 12, pp. 8052–8066, Dec. 2017.
- [16] Y. Zhu, G. Zheng, and M. Fitch, "Secrecy rate analysis of uav-enabled mmwave networks using matern hardcore point processes," *IEEE J. Sel. Areas Commun.*, vol. 36, no. 7, pp. 1397–1409, Jul. 2018.
- [17] L. Wei, R. Q. Hu, Y. Qian, and G. Wu, "Key elements to enable millimeter wave communications for 5G wireless systems," *IEEE Wireless Commun.*, vol. 21, no. 6, pp. 136–143, Dec. 2014.
- [18] S. N. Chiu, D. Stoyan, W. S. Kendall, and J. Mecke, *Stochastic Geometry and Its Applications*, 3rd ed. New York: John Wiley and Sons, Inc., 2013.
- [19] M. Haenggi, *Stochastic Geometry for Wireless Networks*, 1st ed. Cambridge University Press, 2012.
- [20] A. Al-Hourani, S. Kandeepan, and S. Lardner, "Optimal LAP altitude for maximum coverage," *IEEE Wireless Commun. Lett.*, vol. 3, no. 6, pp. 569–572, Dec. 2014.
- [21] C.-H. Liu and L.-C. Wang, "Optimal cell load and throughput in green small cell networks with generalized cell association," *IEEE J. Sel. Areas Commun.*, vol. 34, no. 5, pp. 1058–1072, May 2016.
- [22] C.-H. Liu, "Coverage-rate tradeoff analysis in mmwave heterogeneous cellular networks," *IEEE Trans. Commun.*, vol. 67, no. 2, pp. 1720–1736, Feb. 2019.
- [23] M. Akdeniz, Y. Liu, M. Samimi, S. Sun, S. Rangan, T. Rappaport, and E. Erkip, "Millimeter wave channel modeling and cellular capacity evaluation," *IEEE J. Sel. Areas Commun.*, vol. 32, no. 6, pp. 1164–1179, Jun. 2014.
- [24] C.-H. Liu and L.-C. Wang, "Random cell association and void probability in poisson-distributed cellular networks," in *IEEE Int. Conf. on Commun.*, Jun. 2015, pp. 2816–2821.
- [25] T. Bai and R. W. Heath, "Coverage and rate analysis for millimeter-wave cellular networks," *IEEE Trans. Wireless Commun.*, vol. 14, no. 2, pp. 1100–1114, Feb. 2015.
- [26] C.-H. Liu and H.-C. Tsai, "Traffic management for heterogeneous networks with opportunistic unlicensed spectrum sharing," *IEEE Trans. Wireless Commun.*, vol. 16, no. 9, pp. 5717–5731, Sep. 2017.
- [27] F. Baccelli and B. Błaszczyszyn, "Stochastic geometry and wireless networks: Volume I Theory," *Foundations and Trends in Networking*, vol. 3, no. 3-4, pp. 249–449, 2010.
- [28] D. P. Bertsekas, *Nonlinear Programming*, 3rd ed. Belmont, MA: Athena Scientific, 2016.